HEALTH AND MEDICINE

Proof of concept for rational design of hepatitis C virus E2 core nanoparticle vaccines

Linling He[1]*, Netanel Tzarum[1]*, Xiaohe Lin[1], Benjamin Shapero[1], Cindy Sou[1], Colin J. Mann[1], Armando Stano[1], Lei Zhang[1], Kenna Nagy[2], Erick Giang[2], Mansun Law[2†], Ian A. Wilson[1,3†], Jiang Zhu[1,2†]

Hepatitis C virus (HCV) envelope glycoproteins E1 and E2 are responsible for cell entry, with E2 being the major target of neutralizing antibodies (NAbs). Here, we present a comprehensive strategy for B cell–based HCV vaccine development through E2 optimization and nanoparticle display. We redesigned variable region 2 in a truncated form (tVR2) on E2 cores derived from genotypes 1a and 6a, resulting in improved stability and antigenicity. Crystal structures of three optimized E2 cores with human cross-genotype NAbs (AR3s) revealed how the modified tVR2 stabilizes E2 without altering key neutralizing epitopes. We then displayed these E2 cores on 24- and 60-meric nanoparticles and achieved substantial yield and purity, as well as enhanced antigenicity. In mice, these nanoparticles elicited more effective NAb responses than soluble E2 cores. Next-generation sequencing (NGS) defined distinct B cell patterns associated with nanoparticle-induced antibody responses, which target the conserved neutralizing epitopes on E2 and cross-neutralize HCV genotypes.

INTRODUCTION

Hepatitis C virus (HCV) infects 1 to 2% of the world population and poses a major health burden that leads to ~500,000 deaths annually and an estimated 1.5 to 2 million new infections each year (*1*). The opioid epidemic, causing more than 70,000 overdose-related deaths in 2017 alone, has directly contributed to the rapid rise of HCV infection in North America (*2*). Most HCV patients (75 to 85%) will develop a chronic infection resulting in hepatocellular carcinoma, cirrhosis, and other severe liver diseases (*1*). While direct-acting antiviral (DAA) therapies have increased the cure rate among patients with chronic HCV (*3*), critical challenges remain. First, because HCV infection is asymptomatic, diagnosis often occurs at a late stage after permanent liver damage (*4*). Furthermore, DAA treatment cannot prevent HCV reinfection or reduce the risk of liver cancer for patients with advanced liver disease (*5*, *6*). In addition, the emergence of DAA-resistant strains in patients could eventually render these antivirals ineffective. Increased HCV-associated mortality and new infections (*2*, *7*) in injection drug users highlight the urgent need to develop an effective prophylactic vaccine to combat HCV.

One of the challenges for HCV vaccine development is how to elicit a broadly protective immune response to overcome the high genetic diversity of six major genotypes and more than 86 subtypes (*8*). Moreover, rapid mutation of HCV leads to viral quasispecies that can escape the immune response in infected individuals (*9*). Notwithstanding, spontaneous viral clearance in 20 to 30% of acutely infected patients suggests that chronic HCV infection is preventable if an effective memory response can be established upon vaccination. Glycoproteins E1 and E2 form a heterodimer on the HCV envelope that mediates viral entry into host hepatocytes (*10*). E2 interacts with host cellular receptors CD81 and SR-B1 (*11*) and is a major target for neutralizing antibodies (NAbs), which counteract HCV primarily by blocking CD81 interactions (*12*). Crystal structures of an E2 core (E2c) derived from isolate H77 (genotype 1a) in complex with a broadly neutralizing antibody (bNAb), AR3C, and a truncated E2 derived from isolate J6 (genotype 2a) bound to a non-NAb, 2A12, provided the first insight into immune recognition of HCV envelope glycoproteins and paved the way for structure-based design of antiviral drugs and vaccines (*13*, *14*). Diverse vaccine strategies such as viral vectors, DNA vaccines, virus-like particles (VLPs), and recombinant E2 and E1E2 proteins have been explored (*15*), but so far, no licensed vaccine is available to prevent HCV infection. Although recombinant E1, E2, and E1E2 glycoproteins have elicited NAb responses in animals and humans (*16*), neutralization breadth was limited and the response was directed mainly to those immunodominant variable loops. Therefore, HCV vaccine efforts should be focused on the design and optimization of envelope glycoprotein immunogens capable of eliciting a bNAb response.

Over the past decade, several rational design strategies have been proposed and validated in vaccine development for HIV-1, including epitope-focused (*17*, *18*) and native trimer-based approaches (*19*, *20*). Despite their differences in design details, these vaccine strategies aim to direct the immune response to bNAb epitopes by grafting an epitope onto heterologous scaffolds, removing or suppressing immunodominant regions, and stabilizing antigen structures. Another important advance in the HIV-1 vaccine field was the development of self-assembling protein nanoparticles to present stabilized gp140 trimers and epitope scaffolds as multivalent, VLP-type vaccines (*21*–*25*). These general design principles and nanoparticle platforms can, in principle, be applied to a wide range of vaccine targets including HCV. Epitope scaffolds have been designed for conserved E1 and E2 NAb epitopes (*26*–*28*) but with no reported in vivo data or little improvement in neutralization breadth. Recent crystal structures of partial E2 ectodomain ($E2_{ECTO}$)—without hypervariable region 1 (HVR1) and stalk region—in complex with NAbs HEPC3 and HEPC74 indicate that variable loops may occlude antibody access to conserved neutralizing epitopes on E2 or E1E2 interface (*29*).

[1]Department of Integrative Structural and Computational Biology, The Scripps Research Institute, La Jolla, CA 92037, USA. [2]Department of Immunology and Microbiology, The Scripps Research Institute, La Jolla, CA 92037, USA. [3]Skaggs Institute for Chemical Biology, The Scripps Research Institute, La Jolla, CA 92037, USA.
*These authors contributed equally to this work as co-first authors.
†Corresponding author. Email: mlaw@scripps.edu (M.L.); wilson@scripps.edu (I.A.W.); jiang@scripps.edu (J.Z.)

Here, we designed self-assembling E2 core nanoparticles and assessed their potential as HCV vaccines. We first performed ensemble-based de novo design for the truncated VR2 (tVR2) of an E2 core derived from isolate H77 (genotype 1a) and extended the best tVR2 design to an E2 core derived from isolate HK6a (genotype 6a). The optimized E2 mini-cores (termed E2mc3) and E2mc3 variants (v1-v10) demonstrated greater antigenicity and thermostability than E2c3, our previous E2 core construct (*30*). Crystal structures of three E2mc3 variants derived from two genotypes in complex with bNAb AR3C or AR3B revealed how the redesigned tVR2 stabilizes E2 structure and the conformational plasticity of the E2 front layer (FL) region. We then displayed selected E2mc3 variants on ferritin (FR) (24-mer), E2p (60-mer), and I3-01 (60-mer) nanoparticle platforms, which have been used to present diverse HIV-1 and HCV antigens (*21*, *22*, *24*, *26*). These E2 core nanoparticles demonstrated high yield, high purity, and enhanced antigenicity with respect to individual E2 cores. Last, we performed a mouse study to determine the immune responses elicited by different vaccine constructs. Overall, nanoparticles induced high titers of E2-specific antibodies with greater potency and breadth than E2 cores. Next-generation sequencing (NGS) analysis of E2-specific B cells revealed distinct patterns associated with E2 core and nanoparticle vaccines. Significant differences were found between E2 core and nanoparticle in serum NAb response and B cell pattern. Epitope mapping indicated that nanoparticle induced more effective NAb responses to the FL and antigenic site 412 (AS412). Our proof-of-concept study thus presents a B cell–based HCV vaccine strategy and a set of E2 core nanoparticles as potential vaccine candidates.

RESULTS

Structure-based optimization of HCV envelope glycoprotein E2 core

The HCV $E2_{ECTO}$ is stabilized by nine conserved disulfide bonds; contains three VRs including hypervariable region 1 (HVR1; amino acids 384 to 410), VR2 (amino acids 460 to 485), and VR3 (amino acids 572 to 597), and is covered with ~11 N-linked glycans (Fig. 1A) (*31*). Although the function of VR2 and VR3 remains unclear, HVR1 is known to modulate SR-BI interaction (*32*) and to facilitate host immune evasion by generating escape mutations and shielding neutralizing epitopes (*33*). Empirical engineering (fig. S1A) has enabled the structure determination of E2 cores (*13*, *14*). By shortening N/C termini and VR2 and by removing glycans at N448 and N576, Kong *et al.* (*13*) obtained the first crystal structure of H77 E2 core (E2c) in complex with bNAb AR3C. Additional truncation at VR3 and its immediate downstream region led to the E2c3 construct (*30*) and crystal structures of HK6a E2c3 bound to bNAbs AR3A/B/D (*34*). These structures revealed an E2 core constituted by a central immunoglobulin (Ig)–like β-sandwich with front and back layers (fig. S1B, left) (*13*). The CD81 receptor binding site is a hydrophobic patch formed by the FL and the CD81 binding loop and overlaps the E2 neutralizing face (fig. S1B, middle) (*35*). However, these current E2 core constructs, E2c and E2c3, exhibit high flexibility involving the C terminus of the FL, the shortened VR2 loop, and the N terminus of the β-sandwich.

Here, we redesigned the VR2 disordered region (amino acids 452-494) to improve E2 core stability. This region is anchored to the back layer and the β-sandwich by two disulfide bonds, C452-C620 and C494-C564 (Fig. 1, A and B). Although this region consists of 43 residues in wild-type E2 and 21 residues in E2c/E2c3, the Cα distance between C452 and C494 is 26.3 Å for H77 E2c (fig. S1B), which could be joined using a minimum of seven residues. To allow some degree of flexibility, we first manually truncated the VR2 loop region to 13 residues, termed tVR2 (Fig. 1, A and B, and fig. S1A). Notably, the tip (amino acids 543 to 546) of the β-sandwich loop (amino acids 540 to 552) was also truncated to focus immune response to bNAb epitopes, because non-NAbs, such as AR1B, E1, and HEPC46, bind to this region (*34*, *36*, *37*). The crystal structure of HK6a E2c3 in complex with non-NAb E1 confirms the role of the β-sandwich loop in E1 recognition (fig. S1, C to E, and table S1). The new E2 core derived from E2c3, with tVR2 and truncated β-sandwich loop, was termed E2mc3. Next, we redesigned tVR2 of H77 E2mc3 for two loop lengths, 13 amino acids (as in E2mc3) and 12 amino acids, using an ensemble-based de novo protein design method (*38*) to identify the optimal tVR2 sequences that stabilize E2mc3 (Fig. 1B). For each tVR2 length, a large ensemble of loop conformations (1000) was generated to connect C452 and C494 (fig. S1F), with Cα root mean square fluctuation (RMSF) ranging from 1.9 to 9.8 Å (average, 3.6 Å) and 1.6 to 7.8 Å (average, 3.2 Å) for the tVR2 loops of 13 and 12 amino acids, respectively (fig. S1G). After extensive Monte Carlo sampling, the five top-ranking sequences for each loop length, named E2mc3-v1-v5 and v6-v10 (Fig. 1B, right, and fig. S1H), were selected for further characterization. As HK6a E2c3 and H77 E2c shared high structural similarity and disordered regions at the C terminus of the FL and the N terminus of the β-sandwich when bound to AR3 bNAbs (*34*), we speculated that the same E2 core design may be applied to both isolates. On the basis of sequence alignment (fig. S1I), we designed HK6a E2mc3 and E2mc3-v1 constructs by adopting the tVR2 sequences and the β-sandwich loop deletion from H77 without further modification. Together, all 11 H77 E2mc3 variants and two HK6a E2mc3 variants were advanced to experimental evaluation.

Biochemical, biophysical, and antigenic assessment of HCV E2mc3 designs

Previously, we extensively characterized our HIV-1 trimer and nanoparticle designs to facilitate immunogen selection for in vivo evaluation (*21*, *22*, *38*). Here, we followed a similar strategy to characterize 13 E2mc3 constructs derived from H77 and HK6a, along with two parental E2c3 constructs (*30*, *34*). All E2 core constructs were transiently expressed in human embryonic kidney (HEK) 293 F cells and purified using an AR3A affinity column (*13*) followed by size exclusion chromatography (SEC) on a Superdex 75 10/300 column. Overall, the E2mc3 variants, irrespective of the isolate and the tVR2 length, showed greater yield than their respective E2c3 constructs after purification by the AR3A antibody column, ranging from 5.0 to 11.5 mg from 1-liter HEK293 F transfection. In the SEC profiles, AR3A-purified E2mc3 protein was mostly in the monomeric form (at 10 ml), with a small peak (at 8.5 ml) indicative of aggregates (Fig. 1C and fig. S2A). SEC-purified E2mc3 and E2c3 proteins ran as a single band (~50 kDa) in SDS–polyacrylamide gel electrophoresis (SDS-PAGE) (Fig. 1D and fig. S2B). We then tested H77 and HK6a E2mc3 variants by enzyme-linked immunosorbent assay (ELISA) with a large panel of HCV-specific antibodies. This antibody panel consists of eight bNAbs targeting the major E2 neutralizing epitopes (*35*) such as AS412, AS434, and antigenic region 3 (AR3); one NAb (AR2A); and three non-NAbs that recognize AR1 (fig. S2C). H77 E2mc3 showed greater binding affinity than E2c3 for most bNAbs (excluding HEPC3/74) and for NAb AR2A, with further improvement

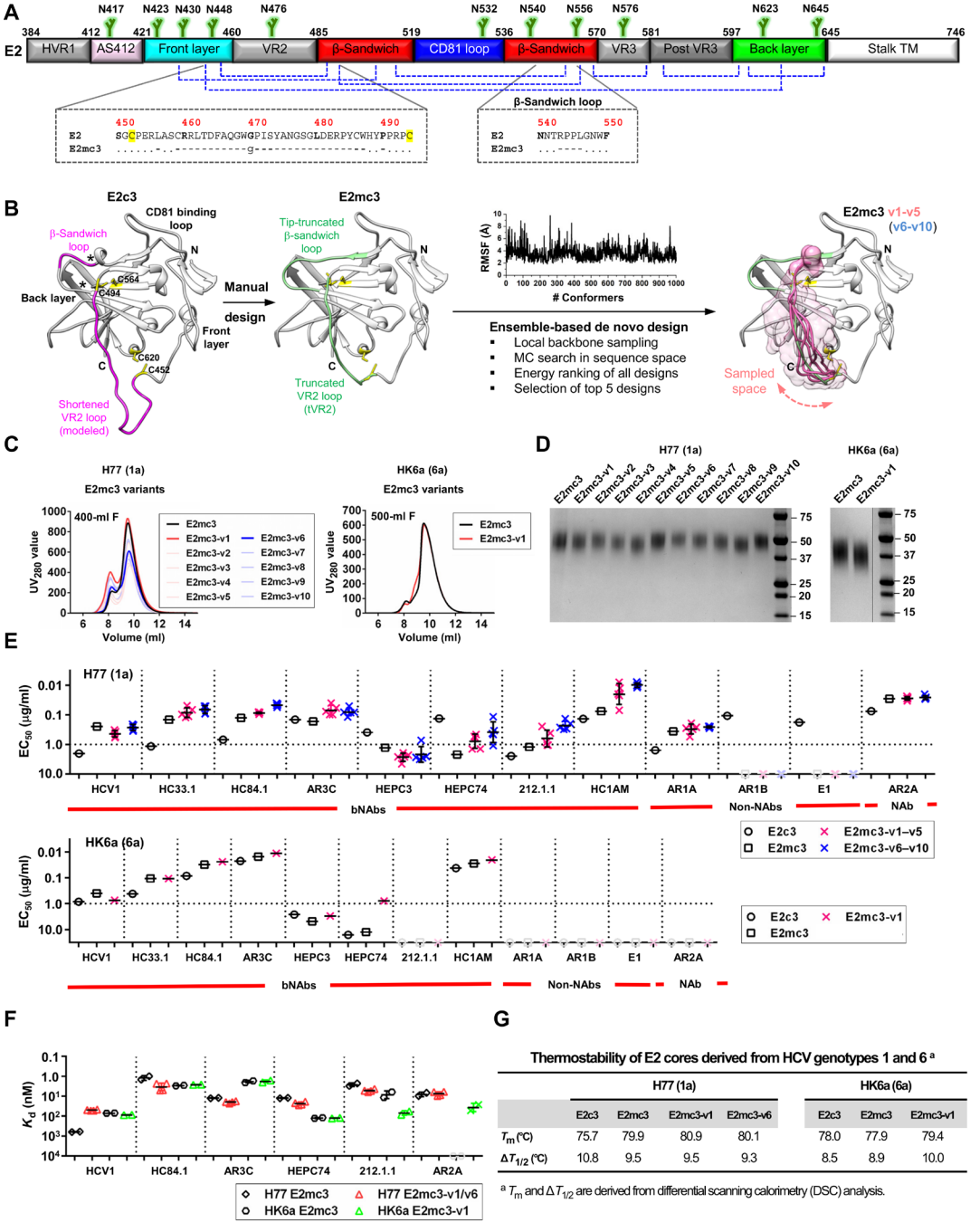

Fig. 1. Rational design of HCV E2 cores. (**A**) Schematic representation of HCV E2 (amino acids 384 to 746) colored by structural components with VRs in gray, AS412 in pink, FL in cyan, β-sandwich in red, CD81 binding loop in blue, back layer in green, and stalk transmembrane (TM) region in white, and N-linked glycans and conserved disulfide bonds are indicated by green branches and blue dashed lines, respectively. Sequence alignment of the design regions between E2 and E2mc3 is shown below. (**B**) Structure-based design of E2 mini-cores. Left: Structure of H77 E2c3 (modeled upon H77 E2c in PDB ID: 4MWF) with shortened VR2 loop modeled by LOOPY. The re-designed β-sandwich loop and the shortened VR2 loop are colored in magenta. Disulfide bonds, C494-C564 and C452-C620, which anchor the VR2 loop to the back layer, are shown in yellow sticks. FL, CD81 binding loop, and back layer are also labeled. Middle 1: Structure of H77 E2mc3 with tip-truncated β-sandwich loop and further tVR2 loop is colored in green. Middle 2: RMSF plot for redesigned tVR2 ensemble is shown with the major steps involved in the ensemble-based de novo protein design below. Right: Structure of H77 E2mc3 with five top-ranking tVR2 design variants (E2mc3 v1-v5) colored in pink and highlighted in a transparent molecular surface. (**C**) SEC profiles of E2mc3 and variants. Left: H77 E2mc3 (in black), v1-v5 (v1 in red and v2-v5 in light red), and v6-v10 (v6 in blue and v7-v10 in light blue). Right: HK6a E2mc3 (in black) and v1 (in red). (**D**) SDS-PAGE of E2mc3 and variants (left, H77; right, HK6a). (**E**) EC_{50} (μg/ml) values of H77 (top) and HK6a (bottom) E2 cores binding to 12 HCV antibodies, including 8 bNAbs (HCV1, HC33.1, HC84.1, AR3C, HEPC3, HEPC74, 212.1.1, and HC1AM), 1 NAb (AR2A), and 3 non-NAbs (AR1A, AR1B, and E1). E2 cores tested here include E2c3, E2mc3, and E2mc3 variants (10 for H77 and 1 for HK6a). (**F**) Binding affinities [dissociation constant (K_d) values in nM] of H77 and HK6a E2mc3 variants for six selected HCV antibodies. (**G**) Thermal stability of H77 and HK6a E2c3 and E2mc3 variants measured by DSC. Two thermal parameters, T_m and $\Delta T_{1/2}$, are listed for four H77 E2 cores and three HK6a E2 cores.

observed for some E2mc3 variants (Fig. 1E, top, and fig. S2, D and E). Although tVR2 does not overlap with the HEPC3/74 epitopes (*29*), the length and sequence of tVR2 appeared to have a notable effect on HEPC3/74 binding. As expected, the truncation of the β-sandwich loop resulted in reduced binding to non-NAbs AR1B and E1 with negligible effect on AR1A, which does not interact with the β-sandwich loop (*36*). Similar patterns were observed for HK6a E2mc3 and E2mc3-v1 except for NAb 212.1.1 (Fig. 1E, bottom, and fig. S2, F and G) (*39*). However, no detectable binding to AR2A and AR1A/B was observed, as these antibodies are genotype specific (*36*). The antigenicity of E2mc3 and selected variants (v1 and v6 for H77 and v1 for HK6a) was further characterized by biolayer interferometry (BLI) using a set of representative antibodies (Fig. 1F and fig. S2, H to J). In brief, H77 and HK6a E2mc3 variants exhibited similar antigenic profiles with improved bNAb recognition and reduced binding to non-NAbs that target the β-sandwich loop. Last, we determined the thermostability of E2mc3 and variants using differential scanning calorimetry (DSC) (Fig. 1G and fig. S2K). H77 E2mc3 showed a 4.2°C increase in the thermal denaturation midpoint (T_m) relative to E2c3, supporting the notion that truncating VR2 improves E2 core stability. Computational redesign of tVR2 further increased T_m by 1° and 0.2°C for H77 E2mc3-v1 and v6, respectively. In addition, the notable 1.3° to 1.5°C reduction in the temperature transition width ($\Delta T_{1/2}$) indicated a more cooperative unfolding transition for the redesigned H77 E2 cores. HK6a E2mc3-v1 exhibited greater thermostability than E2c3 with a moderate increase in $\Delta T_{1/2}$, which suggests an adversary effect upon incorporation of the tVR2 loop designed for H77.

Structural characterization of minimized cores derived from H77 and HK6a

We next determined the structures of selected E2mc3 variants to investigate whether they can retain the native E2 core conformation with minimal perturbations to the neutralizing epitopes (fig. S2C). Crystallization of H77 and HK6a E2 cores with Fabs derived from bNAbs AR3A/B/C/D led to structures of H77 E2mc3-v1 and E2mc3-v6 in complex with AR3C and HK6a E2mc3-v1 with AR3B at 1.90, 2.85, and 2.06 Å, respectively (Fig. 2 and table S2). The overall fold of E2mc3 variants is highly similar to that of H77 E2c and HK6a E2c3 [Protein Data Bank (PDB): 4MWF and 6BKB] (Fig. 2A) but with notable differences in the C-terminal part of the back layer (amino acids 629 to 640) (*34*) and in an FL loop (amino acids 430 to 438) (fig. S3A) that connects β1 and α1 (*13*) and interacts with the HCDR3 (heavy-chain complementarity-determining region 3) loops of bNAbs AR3A/B/C/D. Structural superposition of E2mc3 variants onto H77 E2c and HK6a E2c3, all in their bNAb-bound states, indicates that this loop adopts a different conformation in each complex yet maintains similar hydrophilic contacts with HCDR3 (fig. S3A), further supporting the conformational plasticity of the E2 FL (*30*). The high-resolution structures also shed some light on how the two design components—β-sandwich loop shortening and VR2 truncation/redesign—affects epitopes on E2. The shortened β-sandwich loop can be fully modeled in the structure of H77 E2mc3-v1 in complex with bNAb AR3C (fig. S3B). Superposition of AR3C-bound H77 E2mc3-v1 onto non–NAb E1–bound HK6a E2c3 confirmed that the β-sandwich loop truncation results in the loss of key interactions with non-NAb E1, consistent with the ELISA data (Fig. 1E and fig. S2D). The redesigned tVR2 can be fully modeled in the bNAb-bound H77 and HK6a E2mc3-v1 structures but is only partially visible in the AR3C-bound H77 E2mc3-v6 structure (Fig. 2C and fig. S4A). Structural analysis confirmed that tVR2 redesign does not introduce any conformational change to the neutralizing face in the context of an E2 core (Fig. 2D). The redesigned tVR2s is anchored to the back layer and the β-sandwich by disulfides bonds C452-C620 and C494-C564 and interacts with the truncated VR3 and the β-sandwich (fig. S4B). While H77 and HK6a E2mc3-v1 constructs share the same tVR2 sequence, a significant difference in the tVR2 conformation was observed (Fig. 2C and fig. S4C), likely resulting from differences in sequence and structure of the adjacent VR3 and β-sandwich loop (*34*) in genotypes 1 and 6 (figs. S3B and S4C). Recently, Flyak *et al.* (*29*) reported the crystal structures of $E2_{ECTO}$ (without HVR1 and stalk) derived from genotype 1 isolates 1a53 and 1b09 in complex with bNAbs HEPC3/74. The full-length VR2 in these structures (figs. S1A and S4D) appears to form a variable face that folds around VR3 (*29*). These new structures allowed us to examine the redesigned tVR2 in the context of a more complete E2. Superposition of H77 E2mc3-v1 onto 1a53 and 1b09 $E2_{ECTO}$ confirmed that tVR2 redesign had little effect on the E2 neutralizing face. Together, the results demonstrate that E2c/E2c3 can be further minimized to improve stability and antigenicity while retaining an intact, native-like core structure in comparison with E2s containing full-length VR2 and VR3 (*29*).

Design and characterization of nanoparticles presenting optimized E2 cores

VLPs can induce strong, long-lasting immune responses and have been used as vaccines against cognate viruses or as carriers of foreign antigens (*40*, *41*). In a recent study, HCV E2 and E2c were incorporated into interbilayer cross-linked multilamellar vesicles, which elicited a genotype-specific NAb response in mice (*42*). Self-assembling protein nanoparticles may provide more desirable vaccine carriers than lipid vesicles owing to their well-defined size, symmetry, and surface density. Through rational design and gene fusion, protein nanoparticles have been used to display diverse antigens such as HIV-1 envelope trimers and scaffolded HIV-1 and HCV bNAb epitopes (*21*–*24*, *26*). Recently, Yan *et al.* (*43*) reported improved immunogenicity in mice for an FR nanoparticle carrying soluble E2 (sE2; amino acids 384 to 661), which contains three full-length immunodominant variable loops. However, the evolutionary conservation of FR across all forms of life (*44*) may limit its use as a carrier for human vaccines.

In this study, we displayed our E2mc3 variants, which only present the conserved bNAb epitopes, on self-assembling protein nanoparticles as multivalent HCV vaccine candidates (Fig. 3A). We tested three nanoparticle platforms, 24-meric FR as a control and 60-meric E2p and I3-01, which range from 12.2 to 25.0 nm and increase in size to 24.5 to 37.5 nm when decorated with E2mc3-v1 (Fig. 3B). E2p and I3-01 are two hyperstable nanoparticles of bacterial origin that have been used to display HIV-1 Env trimers with enhanced antigenicity and immune response (*21*, *22*). Here, we genetically fused the C terminus of E2mc3-v1 to the N terminus of a nanoparticle subunit via a 10-residue linker, $(G4S)_2$, termed 10GS. The six constructs were transiently expressed in 50 ml of ExpiCHO (FR and I3-01) or 2-liter HEK293 F (E2p) cells and purified on an AR3A antibody column followed by SEC on a Superose 6 10/300 GL column (Fig. 3C and fig. S5A). The yield ranged from ~0.5 mg (1-liter HEK293 F cells) to ~20 mg (1-liter ExpiCHO cells) after AR3A processing. For H77, the SEC profiles demonstrated substantial yield and purity for all E2

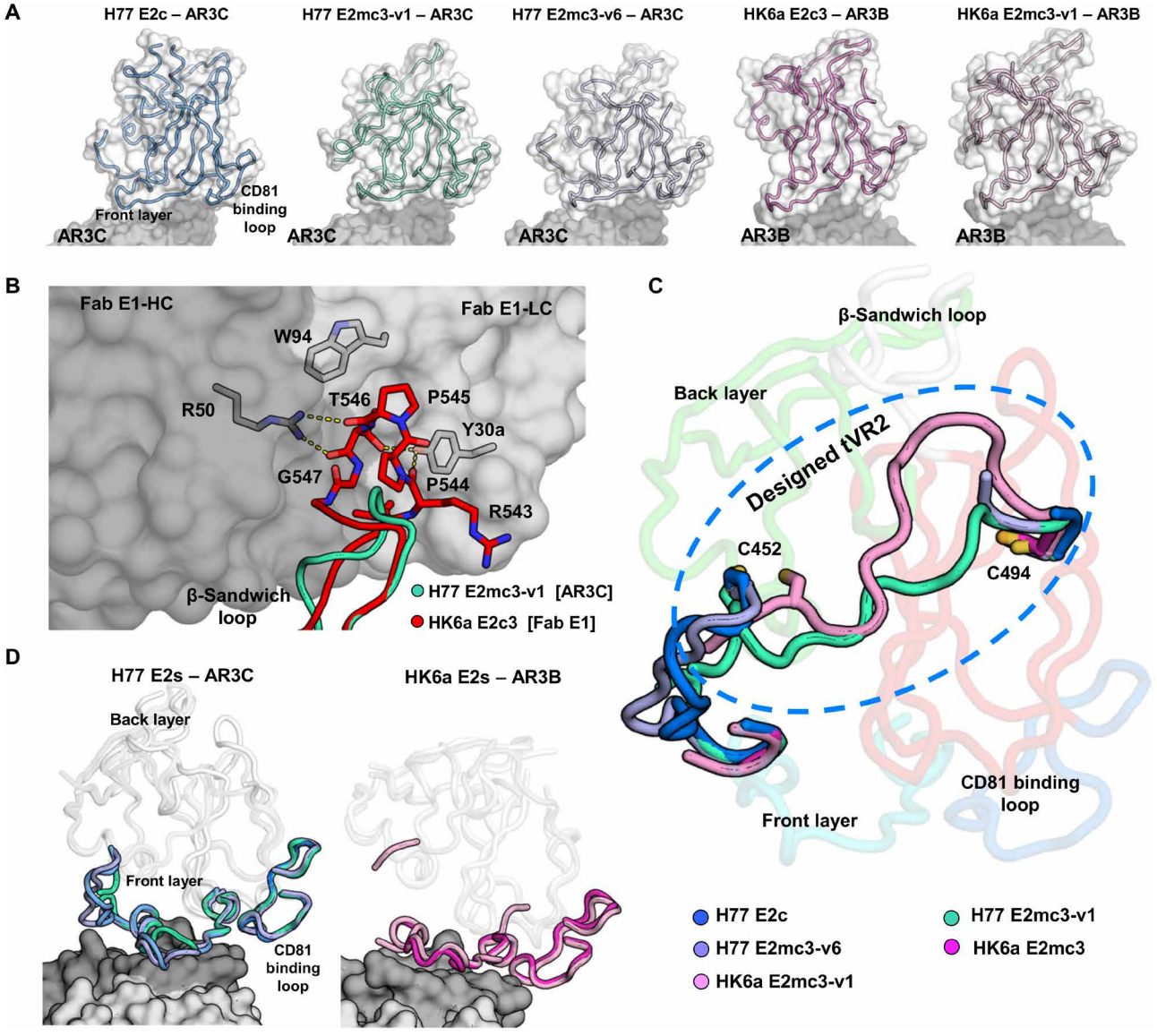

Fig. 2. Structures of rationally designed HCV E2 cores. (**A**) Crystal structures of H77/HK6a E2mc3 indicate an overall similar fold to H77 E2c and HK6a E2c3 (PDB: 4MWF and 6BKB). (**B**) Superposition of the β-sandwich loop from the H77 E2mc3-v1 structure on the HK6a E2c3–Fab E1 complex confirms that loss of binding of E2mc3s to Fab E1 results from truncation of the β-sandwich loop. (**C**) Superposition of E2 of HK6a E2c3 (PDB: 6BKB), H77 E2mc3-v1, H77 E2mc3-v6, and HK6a E2mc3-v1 on the structure of H77 E2c (PDB: 4MWF), illustrating the conformation of the redesigned tVR2 (amino acids 452 to 494). The redesigned tVR2 regions of H77 E2mc3-v1 and HK6a E2mc3-v1 structures are fully modeled but only partly in the H77 E2mc3-v6 structure. (**D**) Superposition of the H77/HK6a E2mc3 structures to H77 E2c and HK6a E2c3, indicating similar conformation of the neutralization face with only local conformational changes for the redesigned VR2 E2s.

core nanoparticles with different patterns for 24-mer versus 60-mer. While E2mc3-v1-10GS-FR produced an aggregate peak at 8 to 9 ml, both E2mc3-v1-10GS-E2p and I3-01 showed a monomer peak at 15 to 20 ml, tailing the nanoparticle peak (Fig. 3C). For HK6a, a reduction in nanoparticle yield and purity was accompanied by increased low–molecular weight (MW) species (fig. S5A), suggesting that H77 tVR2 may be less compatible with HK6a and hinders nanoparticle assembly. The SEC-purified protein was analyzed by blue-native PAGE (BN-PAGE) and negative-stain electron microscopy (nsEM), which showed high-MW bands and homogeneous nanoparticles, respectively (Fig. 3, D and E, and fig. S5, B and C). Previously, we reported significantly enhanced bNAb binding to nanoparticle-displayed HIV-1 antigens due to avidity (*21*, *22*, *24*). Here, a similar pattern was observed for HCV E2 core nanoparticles with up to 100-fold change in median effective concentration (EC_{50}) for most bNAbs, whereas binding to non-NAbs that target the β-sandwich loop remained undetectable (Fig. 3F and fig. S5, D to G). Notably, HK6a E2mc3-v1 regained its binding to genotype-specific AR1A and AR2A when displayed on E2p and I3-01 60-mers, which showed differential binding to some bNAbs with up to eightfold variation in EC_{50}, suggesting a nanoparticle-specific preference. In BLI, correlation between peak binding signal and antigen valency was observed irrespective of the E2 genotype, with 60-mers > 24-mers > E2 core (on average) (Fig. 3G and fig. S5, H and I). A similar correlation was

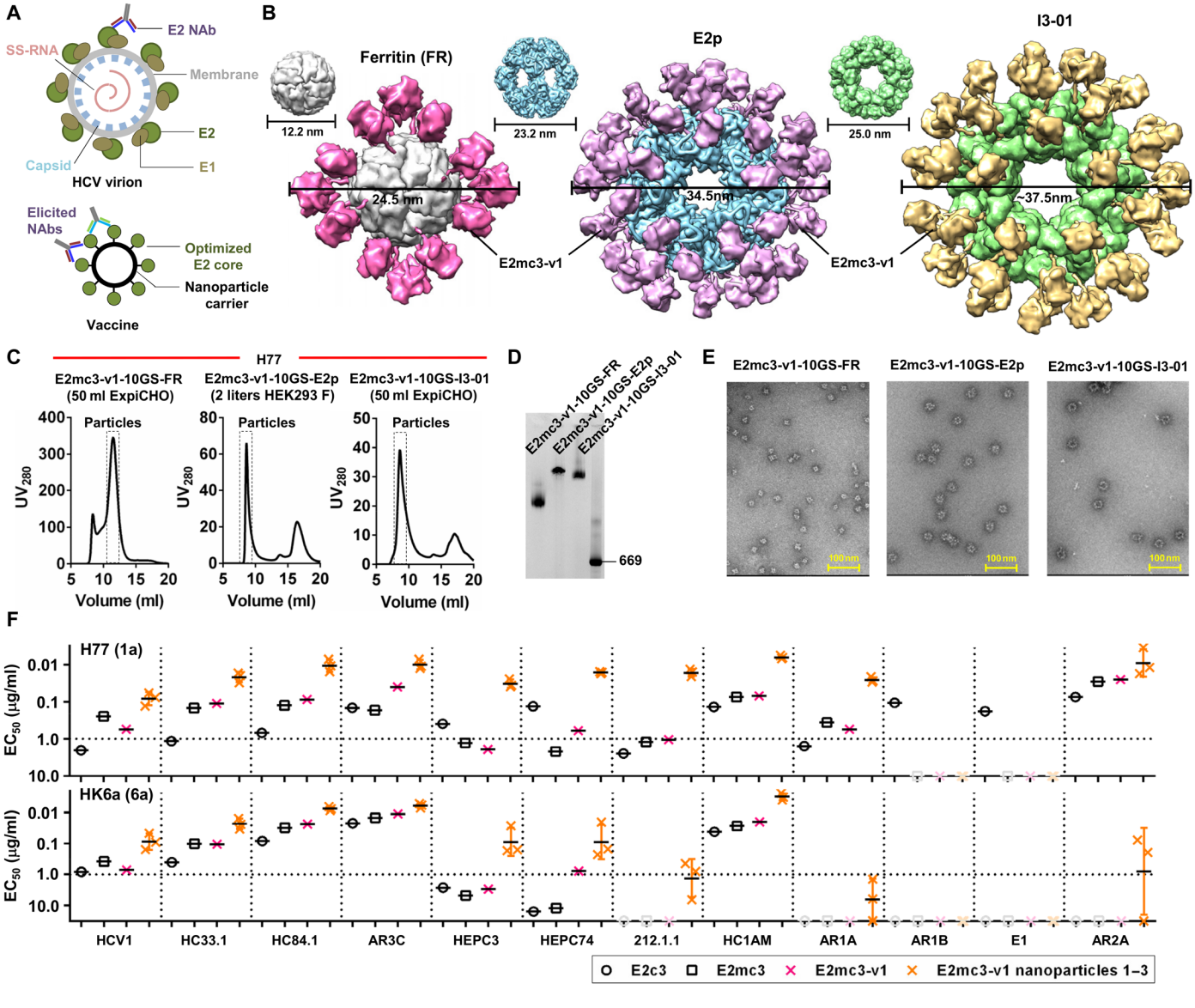

G

E2 core immunogens	HCV1	HC84.1	AR3C	HEPC74	212.1	AR2A	HCV1	HC84.1	AR3C	HEPC74	212.1.1	AR2A
E2mc3-v1	0.23	0.28	0.25	0.35	0.25	0.10	0.19	0.27	0.21	0.19	0.08	0.04
E2mc3-v1-10GS-FR	0.51	1.00	0.93	0.77	0.45	0.80	0.61	1.53	1.37	1.27	0.68	0.19
E2mc3-v1-10GS-E2p	0.53	1.14	1.21	0.97	0.56	1.25	1.12	0.92	1.04	1.60	1.14	0.42
E2mc3-v1-10GS-I3-01	0.89	1.81	1.72	1.44	0.86	1.33	1.15	1.91	1.27	1.77	1.28	0.41

Fig. 3. Rational design of self-assembling E2 core nanoparticles. (**A**) Schematic representation of HCV virion (top) and E2 core–based nanoparticle vaccine (bottom). For the HCV virion, single-stranded RNA (SS-RNA), capsid, membrane, and envelope glycoproteins E1 and E2 are labeled, while for the vaccine, the optimized E2 core and nanoparticle carrier are labeled. (**B**) Colored surface models of nanoparticle carriers (top) and E2 core–based nanoparticle vaccines (bottom). Three nanoparticle carriers shown here are 24-meric FR and 60-meric E2p and I3-01. Nanoparticle size is indicated by diameter (in nanometers). (**C**) SEC profiles of H77 E2mc3-v1 nanoparticles obtained from a Superose 6 10/300 GL column. The particle fraction is indicated by a dotted-line box. While both FR and I3-01 nanoparticles were produced in ExpiCHO cells, E2p nanoparticles were expressed in HEK293 F cells. (**D**) BN-PAGE of SEC-purified H77 E2mc3-v1 nanoparticles. (**E**) nsEM images of SEC-purified H77 E2mc3-v1 nanoparticles. (**F**) EC_{50} (μg/ml) values of H77 (top) and HK6a (bottom) E2mc3-v1 nanoparticles binding to 12 HCV antibodies listed in Fig. 1C. (**G**) Antigenic profiles of H77 (left, in red) and HK6a (right, in green) E2mc3-v1 and three nanoparticles against six HCV antibodies. Sensorgrams were obtained from an Octet RED96 using an antigen titration series of six concentrations (3.57 to 0.11 μM by twofold dilution for E2mc3-v1 and 52.08 to 1.63 nM by twofold dilution for nanoparticles) and quantitation biosensors, as shown in fig. S5 (H and I). The peak signals (in nanometers) at the highest concentration are listed in the matrix. Higher color intensity indicates greater binding signal measured by Octet.

noted for HIV-1 gp140 nanoparticles in our previous study (*21*). Of the two 60-mers, I3-01 showed greater bNAb binding than E2p, suggesting that the large spacing of the N termini (50.5 Å) makes I3-01 more suitable for displaying individual antigens. In summary, these E2 core nanoparticles, presenting 24 or 60 copies of each bNAb epitope on the surface, provide novel vaccine candidates for in vivo evaluation.

E2 core nanoparticles elicit stronger immune responses than E2 cores in mice

Previously, Bazzill *et al.* (*42*) reported improved immunogenicity for H77 E2c-attached lipid vesicles compared to E2c alone, with heterologous neutralization observed for a genotype 1b isolate. Enhanced immunogenicity was also reported for an FR nanoparticle carrying sE2 (*43*). In our previous study, HIV-1 gp140 nanoparticles elicited an emerging tier-2 NAb response in mice and rabbits after 6 to 8 weeks (*21*). Here, we assessed H77 and HK6a E2 core nanoparticles in mouse studies #1 and #2, respectively, using a short regimen where we injected wild-type BALB/c mice four times with a 3-week interval (Fig. 4A). All vaccine antigens (E2 cores and nanoparticles) were formulated with AddaVax, an oil-in-water emulsion adjuvant similar to MF59, which has been used as a vaccine adjuvant in humans including the HCV E1E2 vaccine trial (*45*, *46*). In addition, AddaVax has been used with FR nanoparticles presenting HIV-1 epitope scaffolds and gp140 trimers in our previous studies (*21*, *24*), suggesting that it may be a suitable adjuvant for in vivo comparison of E2 cores and E2 core nanoparticles. Notably, I3-01 constructs were not included due to the difficulties in producing HK6a E2mc3-v1-10GS-I3-01 nanoparticles, as indicated by SEC (fig. S5A). We first performed a longitudinal analysis of serum antibody titers to E2mc3-v1. In study #1, for three H77-based vaccine constructs (Fig. 4B, top, and fig. S6, A and B), a positive correlation between E2-specific EC_{50} titer and antigen valency was observed for week 2, with statistical significance determined by unpaired *t* test ($P < 0.0001$ between E2mc3 and two nanoparticles and $P = 0.0036$ between FR and E2p). While E2-specific antibody titers continued to rise, the differences between three vaccine groups diminished toward the end of the immunization and even slightly reversed in relative titers, with $P \geq 0.0510$ for week 11. In study #2, HK6a E2mc3-v1 and its E2p nanoparticle were compared to a mix of two E2p nanoparticles, one displaying HK6a E2mc3-v1 and the other displaying H77 E2mc3-v1 (Fig. 4B, bottom, and fig. S6, C and D). Equal amounts (1:1 ratio) of H77 and HK6a E2mc3-v1 nanoparticles in solution were mixed before formulation with AddaVax and mouse immunization. The HK6a E2mc3-v1 E2p group retained its advantage in antibody titer only until week 8, whereas its H77 counterpart did until week 11 and showed significant *P* values for three of four time points (weeks 2, 5, and 8) (Fig. 4B, top). The E2p mix elicited significantly higher antibody titers to H77 E2mc3-v1 than to HK6a E2mc3-v1 throughout the immunization, with $P \leq 0.0017$. With half of the dosage corresponding to HK6a, the E2p mix group showed lower antibody titers from week 5 than the E2p group, with significant *P* values observed for weeks 5, 8, and 11 (Fig. 4B, bottom), suggesting a correlation between dosage and antibody titer. Overall, E2 core nanoparticles induced greater antibody titers than E2 cores, although E2 only accounts for 42% (E2p) to 51% (FR) of the protein mass of an E2 core nanoparticle. Thus, when all mice were given the same protein dose, those in the nanoparticle groups received markedly less antigen than their counterparts in the E2 core groups.

We then evaluated serum neutralization using HCV pseudoparticles (HCVpps) (*36*). In study #1, autologous neutralization increased steadily over time with distinct temporal patterns (Fig. 4C, top). At week 2, the FR group showed the highest H77 neutralization, whereas the E2p group was unexpectedly the lowest, contrary to its significant antibody titer at this time point (Fig. 4B, bottom). However, statistical analysis indicated that the difference between FR and the other two vaccine groups was not significant, with *P* values of 0.0683 to 0.5084. Week 5 (after the first boost) appeared to mark a turning point in serum NAb development. From week 5, the FR group showed lower serum neutralization than the other two groups although the difference between the FR and E2mc3-v1 groups was not significant, whereas the E2p group became the best performer at week 8 (after the second boost) with *P* values of 0.0243 (vs. E2mc3-v1) and 0.0088 (vs. FR) and remained more effective than the FR group with a *P* value of 0.0027 at week 11 (after the third boost). The E2p group thus demonstrated a rather moderate advantage in serum neutralization of autologous H77. Week 11 sera also neutralized heterologous isolates HCV-1 (1a), J6 (2), and SA13 (5a), with E2p showing significantly higher HCV-1 and J6 neutralization than the other two groups (Fig. 4C, bottom). This result highlights the ability of E2 core nanoparticles to elicit cross-strain/genotype NAb responses through presentation of the conserved bNAb epitopes to the immune system. For study #2, serum neutralization was assessed against the heterologous H77 HCVpp due to the difficulties in producing high titers of HK6a HCVpp (Fig. 4D). The H77/HK6a E2p mix group and the HK6a-only E2p group showed equivalent H77 neutralization, indicating that the conserved bNAb epitopes on H77 and HK6a E2mc3-v1 can be recognized equally well by murine antibodies (Figs. 1E and 3F). Five HCV bNAbs were used to calibrate the HCVpp neutralization assays, with the HIV-1 bNAb VRC01 (*47*) included as a negative control (Fig. 4E). As expected, all HCV bNAbs exhibited a concentration-dependent pattern, with AR3C being the best neutralizer, whereas VRC01 showed baseline neutralization (<10%) irrespective of the antibody concentration. In summary, serum analysis demonstrated that properly formulated E2 core nanoparticles can induce rapid, high-titer antibody responses that neutralize both autologous and heterologous isolates more effectively than E2 cores. Such an effect was usually more evident at the early time points of the immunization. The overall findings here are reminiscent of our previous study of HIV-1 gp140 nanoparticles (*21*) and suggests that self-assembling protein nanoparticles may provide a general solution for VLP-type vaccine development against diverse viral pathogens.

Distinctive patterns of B cell responses induced by E2 core and E2 core nanoparticle

Previously, we performed NGS to investigate the prevalence of the V_H1-69 germline gene in B cell repertoires of patients with chronic HCV (*34*). We also applied NGS to analyze vaccine-induced B cell response in mice and non-human primates (*21*, *24*, *48*). Here, we combined antigen-specific B cell sorting and antibody NGS to obtain a quantitative readout of vaccine-induced B cell response and determine B cell patterns for different vaccine platforms (Fig. 5A). We first designed an H77 E2mc3-v1 probe with a C-terminal Avi-tag to facilitate E2-specific B cell sorting. This construct was expressed following the same protocol as used for H77 E2mc3-v1, biotinylated, and SEC-purified (fig. S7A), resulting in a probe termed H77 E2mc3-v1-Avi-Biot. We then sorted mouse splenic B cells from two groups

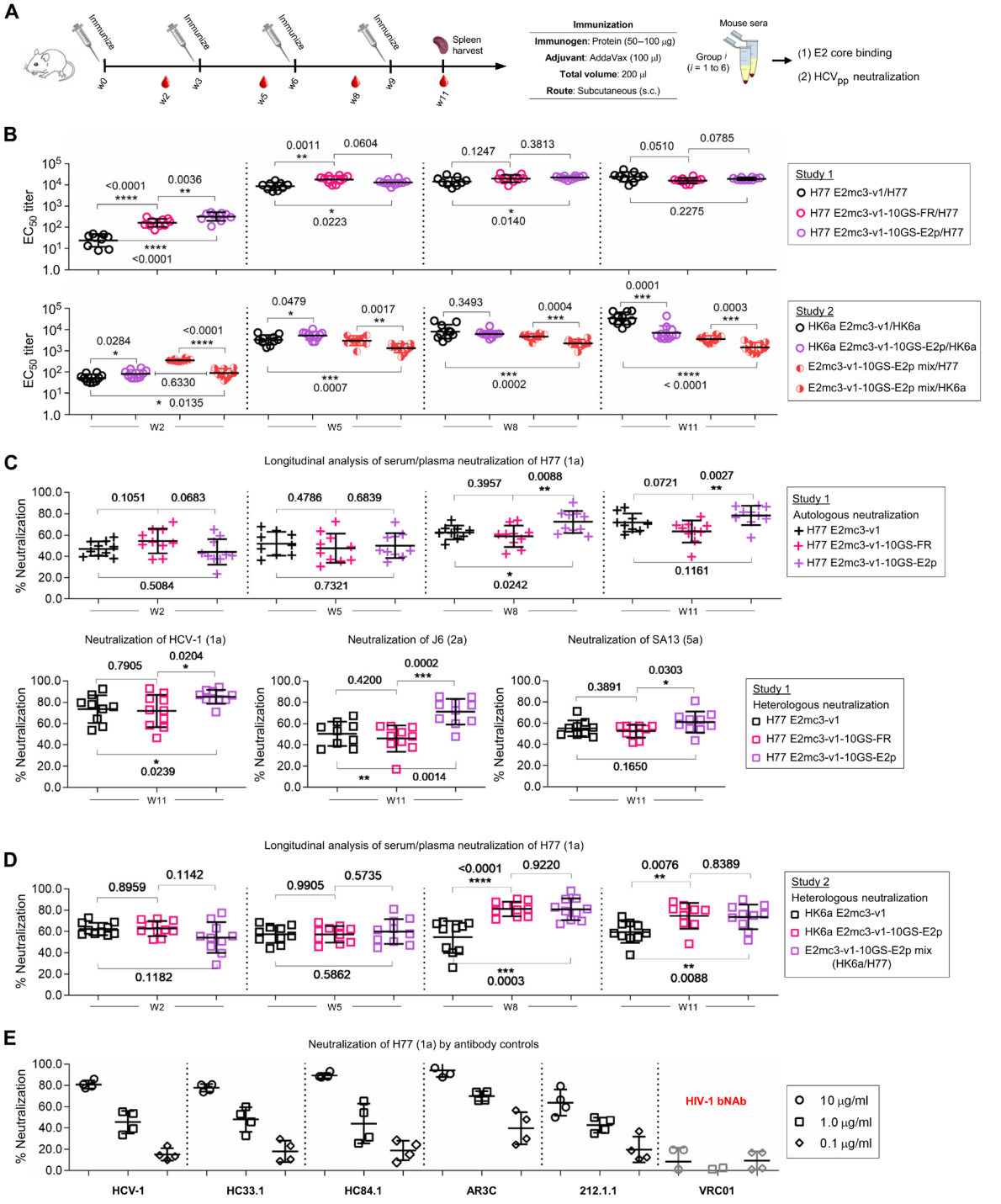

Fig. 4. Immunogenicity of newly designed E2 cores and nanoparticles in mice. (**A**) Schematic representation of the mouse immunization protocol. In study #1, mice were immunized with H77 E2mc3-v1 (group 1), H77 E2mc3-v1-10GS-FR (group 2), and H77 E2mc3-v1-10GS-E2p (group 3). In study #2, mice were immunized with HK6a E2mc3-v1 (group 1), HK6a E2mc3-v1-10GS-E2p (group 2), and HK6a/H77 E2mc3-v1-10GS-E2p mix (group 3). (**B**) Longitudinal analysis of E2-specific antibody titers in immunized mouse sera at weeks 2, 5, 8, and 11. Top: EC_{50} titers (fold of dilution) calculated from ELISA binding of mouse sera in study #1 to the coating antigen, H77 E2mc3-v1. Bottom: EC_{50} titers calculated from ELISA binding of mouse sera in study #2 to the coating antigens HK6a E2mc3-v1 (groups 1–3) and H77 E2mc3-v1 (group 3). Detailed serum ELISA data are shown in fig. S6 (A to D). (**C**) Mouse serum neutralization in study #1. Top: Percent (%) neutralization of mouse sera against autologous H77 at weeks 2, 5, 8, and 11. Bottom: Percent (%) neutralization of mouse sera against heterologous HCV-1, J6, and SA13 at the last time point, week 11, with an advantage in heterologous NAb responses observed for the E2p group. (**D**) Mouse serum neutralization in study #2. Percent (%) neutralization of mouse sera against heterologous H77 at weeks 2, 5, 8, and 11. For (B) to (D), the *P* values were determined by an unpaired, two-tailed Student's *t* test in GraphPad Prism 6 and are labeled on the plots, with (*) indicating the level of statistical significance. (**E**) Validation of the HCVpp neutralization assay using five HCV bNAbs and an HIV-1 bNAb (negative control) against H77. Percent (%) neutralization of all antibodies was determined at three concentrations: 10, 1, and 0.1 μg/ml.

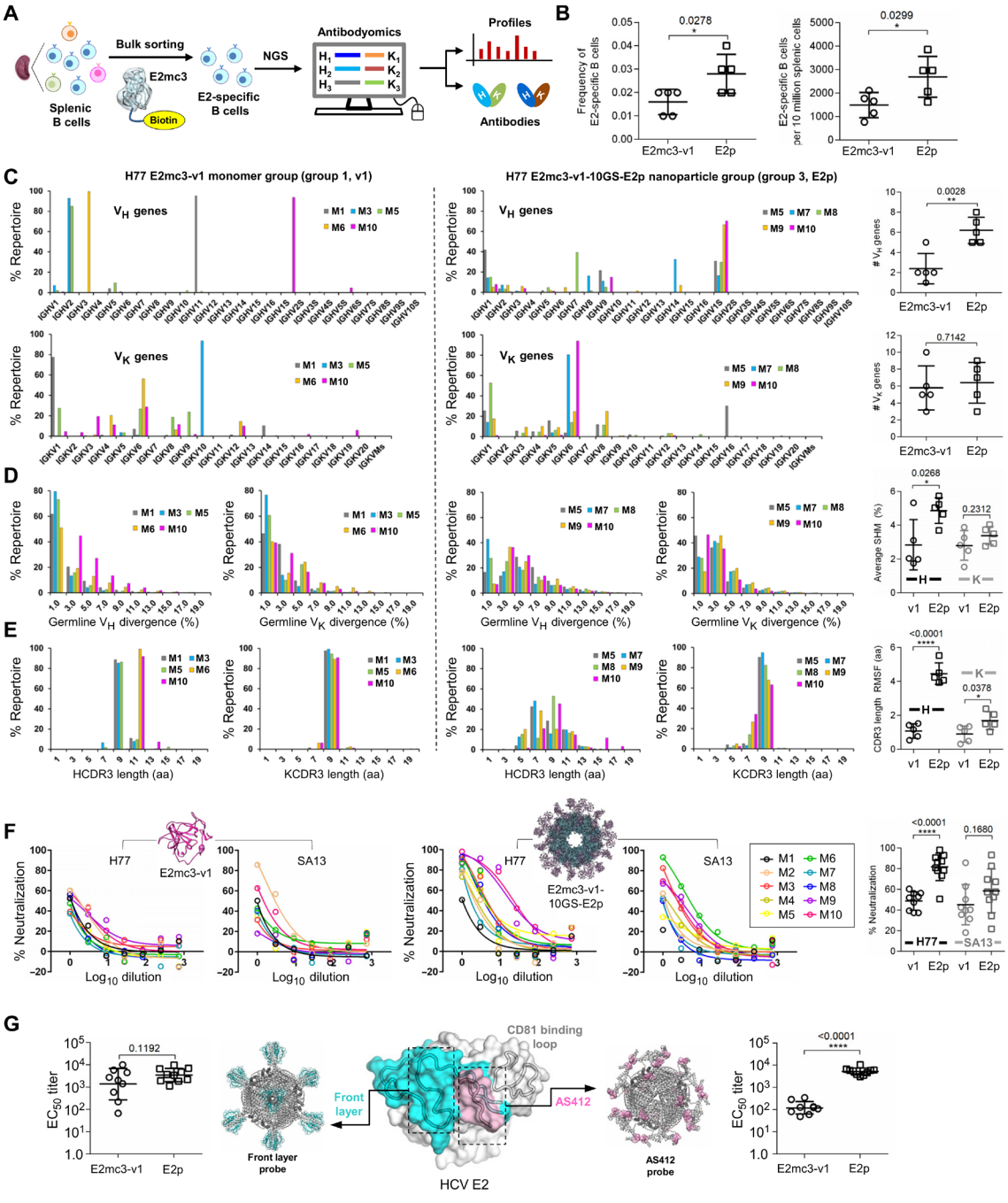

Fig. 5. Patterns associated with HCV E2–specific B cell response in mouse immunization. (**A**) Schematic representation of the strategy used to analyze HCV E2–specific B cell response that combines antigen-specific bulk sorting of splenic B cells with NGS and antibodyomics analysis. (**B**) Statistical analysis of B cell sorting data obtained for group 1 (H77 E2mc3-v1 monomer) and group 3 (H77 E2mc3-v1-10GS-E2p nanoparticle) in study #1. Left: Frequency of E2-specific B cells. Right: Number of E2-specific B cells per million splenic cells. Five mice from group 1 (M1, M3, M5, M6, and M10) and five mice from group 3 (M5, M7, M8, M9, and M10) were randomly selected and analyzed. (**C**) Distribution of germline gene usage plotted for groups 1 and 3. Top: Germline V_H genes. Bottom: Germline V_κ genes. Statistical analysis of number of activated V_H/V_κ genes (≥1% of the total population) is shown on the far right. (**D**) Distribution of germline divergence or degree of SHM plotted for groups 1 and 3. For each group, percent (%) mutation is calculated at the nucleotide level for V_H (left) and V_κ (right). Statistical analysis of germline divergence is shown on the far right. (**E**) Distribution of CDR3 loop length plotted for groups 1 and 3. For each group, CDR3 length calculated at the amino acid (aa) level is shown for heavy (left) and light chains (right). Statistical analysis of RMSF of CDR3 loop length, which is used as an indicator of how much the CDR3 loop length varies within the E2-specific antibodies from each animal. (**F**) Neutralization curves using purified IgG for groups 1 (left) and 3 (right) in study #1. Autologous H77 (1a) and heterologous SA13 (5a) were tested in HCVpp assays with a starting IgG concentration of 100 μg/ml followed by a series of threefold dilutions. Structural models of the immunogens are placed next to their neutralization curves. (**G**) Epitope mapping of polyclonal antibody sera from groups 1 and 3 in study #1. Surface model of $E2_{ECTO}$ is shown in the middle with the FL and AS412 colored in cyan and pink, respectively. Statistical analysis of EC_{50} titers (fold of dilution) of groups 1 and 3 against the FL probe (left) and the AS412 probe (right). Structural models of the designed nanoparticle probes are placed next to their plots. Epitopes on the nanoparticles are colored according to the $E2_{ECTO}$ model. For (B) to (G), statistical analysis was performed using an unpaired, two-tailed Student's *t* test in GraphPad Prism 6 and are labeled on the plots, with (*) indicating the level of statistical significance.

in study #1 immunized with H77 E2mc3-v1 and its E2p nanoparticle. A greater frequency/number of E2-specific B cells was observed for the E2p group with significant *P* values (Fig. 5B and fig. S7B). Sorted B cells from 10 mice, 5 per group, were subjected to library preparation, antibody NGS on Ion GeneStudio S5 (*34*), and repertoire analysis using a mouse antibodyomics pipeline (fig. S7C) (*21*, *24*).

Repertoire profiles revealed distinct patterns associated with the two E2 core vaccines. In terms of germline gene usage, the E2p group used significantly more heavy-chain variable (V_H) genes (five to eight) than the E2mc3-v1 group (about one) in each animal with a *P* value of 0.0084 (Fig. 5C). In contrast, no statistical significance was observed for the usage of κ-chain variable ($V_κ$) genes. In terms of germline divergence or degree of somatic hypermutation (SHM), antibodies elicited by E2p contained more V_H mutations with a *P* value of 0.0268 (Fig. 5D). Although the E2p group showed a higher degree of SHM in Vκ genes, the difference was not significant. Nonetheless, E2p nanoparticle appeared to stimulate B cell maturation more effectively than E2 core. Distinct patterns of HCDR3 length were observed for the two vaccine groups (Fig. 5E). In the E2mc3-v1 group, each mouse showed one predominant HCDR3 length (≥85%), consistent with the highly skewed germline gene usage (Fig. 5C), whereas in the E2p group, a broad range of HCDR3 length was observed for each mouse. To determine the statistical significance of this finding, RMSF was calculated to measure how much the HCDR3 length in each mouse can vary. The E2p group yielded a significantly higher RMSF value than the E2mc3-v1 group, on average, 4.5 amino acids versus 1.1 amino acids, with a *P* value of <0.0001. In contrast, the two vaccine groups showed similar KCDR3 (kappa-chain complementarity-determining region 3) length distributions, both centered around 9 to 11 amino acids (Fig. 5E). Antibody NGS thus revealed the mechanism by which an effective E2 core nanoparticle vaccine can induce potent and broad NAb responses by engaging more naïve B cells, activating diverse germline genes, increasing the rate of V_H somatic mutation, and broadening the range of HCDR3 loop length.

Polyclonal NAbs induced by E2 core and E2 nanoparticle target different epitopes

It has been reported that mouse serum contains nonspecific antiviral activity and interferes with HIV-1 neutralization assays (*49*). The 40 to 80% neutralization observed in mouse serum at week 2 (Fig. 4, B to D) suggested a similar problem for HCVpp neutralization assays. Here, we purified IgG from mouse serum (*21*) in study #1 at week 11 for neutralization of H77 (1a) and SA13 (5a) HCVpps with a starting IgG concentration of 100 μg/ml followed by a series of threefold dilutions (Fig. 5F and fig. S8A). Overall, similar patterns were observed for serum and IgG neutralization (Fig. 5F). For H77, while no mouse sera in the E2mc3-v1 group exhibited >60% neutralization at the first concentration, mice #9 and #10 in the E2p group showed almost plateaued curves, suggesting potent NAbs in the purified mouse IgG. For SA13, the E2p group outperformed the E2mc3-v1 group with a less pronounced difference. Statistical analysis of IgG neutralization data showed significant difference between the E2p group and the E2mc3-v1 group for H77 ($P < 0.0001$), but not for SA13 ($P = 0.1680$). The FR group consistently ranked the lowest in serum neutralization but slightly outperformed the E2mc3-v1 group in IgG neutralization against autologous H77 (fig. S8A). One mouse (#6) in the FR group appeared to have generated potent bNAbs against SA13, as indicated by the neutralization curve (fig. S8A). Nonetheless, our results suggested that FR may not be an optimal nanoparticle platform for HCV vaccine design due to its sequence conservation and low immunogenicity. As a negative control, lymphocytic choriomeningitis virus pseudoparticles (LCMVpps) were tested in IgG neutralization (fig. S8A). Non-specific neutralizing activity against LCMVpp was observed for one mouse in each group. The removal of these two samples in the analysis had no effect on the statistical significance found for H77 neutralization (fig. S8A).

We next mapped the epitopes of the vaccine-induced antibody response. The surface of E2 devoid of HVR1, VR2, and VR3 can be divided into five overlapping immunogenic regions that can be recognized by a panel of human and mouse NAbs (*15*, *35*). Of these, the E2 neutralizing face, which consists of FL (amino acids 421 to 459) and CD81 binding loop (amino acids 519 to 535), and the AS412 (amino acids 412 to 423) are targets of human bNAbs such as the AR3 series (*13*), HC84 series (*50*), HCV1 (*51*), and HC33 series (*52*). Here, two epitope-specific probes were used to examine vaccine-induced antibody responses to FL and AS412 on E2 (Fig. 5G, middle). A trimeric scaffold was designed to present amino acids 421 to 451 of FL, which was anchored to the scaffold backbone via an engineered disulfide bond (fig. S8B, top). This FL scaffold was displayed on the FR nanoparticle to enhance the sensitivity of serum binding. In ELISA, the E2p group yielded an average EC_{50} titer of 4281 compared with 3044 for the E2mc3-v1 group (Fig. 5G, left, and fig. S8C, top). However, unpaired *t* test reported a nonsignificant *P* value of 0.1192 between the two groups (Fig. 5G, left). Nonetheless, nanoparticle display of an optimized E2 core appeared to have improved the recognition of FL, as well as its core element—antigenic site 434 (AS434) (amino acids 434 to 446). We then used a previously designed FR nanoparticle (fig. S8B, bottom) (*26*) to probe the AS412-specific antibody response. In ELISA, the E2p group demonstrated a uniform, robust response to the AS412 β-hairpin with an average EC_{50} titer of 5584, which is 38-fold greater than the E2mc3-v1 group with a significant $P < 0.0001$ (Fig. 5G, right, and fig. S8C, bottom). Our results thus demonstrate how particulate display can focus antibody responses to conserved bNAb epitopes on E2. The two epitope probes used in this analysis also provide valuable tools for assessment of HCV vaccine candidates.

DISCUSSION

The success of DAA therapy for chronic HCV infection has raised questions about the necessity of developing an HCV vaccine. However, issues in DAA treatment have begun to surface, and a prophylactic vaccine is still required to control HCV transmission (*15*, *53*). Although the HCV genetic diversity poses a significant challenge, recent advances in bNAbs and E2 structures have paved the way for new B cell–based vaccine strategies (*15*, *34*, *35*, *54*, *55*).

Here, we presented a novel HCV vaccine strategy that combines E2 optimization and nanoparticle display to stimulate robust B cell response upon vaccination. First, we redesigned the E2 core constructs (*13*, *30*, *34*) for genotypes 1a and 6a by manually truncating VR2 and the β-sandwich loop and computationally optimized the tVR2. VR2 was chosen as the focus of E2 core redesign based on the fact that this variable loop is in close proximity to the E2 neutralizing face in the $E2_{ECTO}$ structure (*29*) and likely involved in immune evasion by shielding conserved bNAb epitopes or posing as a decoy. These new E2 cores not only retained the native-like structure but also showed enhanced thermostability and antigenicity. Next, we displayed these E2 cores on nanoparticles of various sizes that have

been used as carriers for HIV-1 gp140 trimers (*21*, *22*). These E2 core nanoparticles demonstrated high yield, high purity, and enhanced antigenicity. As these E2 core nanoparticles can be expressed in Chinese hamster ovary (CHO) cells and purified by an antibody column, it is possible that they can be produced in an industrial setting under the good manufacturing practice (GMP) standard. Last, mice were immunized with the new E2 core and nanoparticle constructs. Longitudinal serum analysis not only confirmed the superior immunogenicity of E2p-based vaccine constructs but also suggested that FR, which was recently used as a carrier for sE2 (*43*), might require further optimization. NGS analysis of E2-sorted splenic B cells provided much needed insights as to how an effective nanoparticle vaccine can elicit bNAbs with diversified germline gene usage, accelerated antibody maturation, and expanded range of HCDR3 length. Serum analysis with novel probes revealed how particulate display affects epitope recognition by redirecting antibody responses. Notably, quantitative analyses were employed in this study to validate various aspects of the in vivo data, thus providing a rigorous foundation for future comparison of different types of HCV vaccine candidates.

Future investigation should be directed toward several possibilities. First, the suboptimal in vitro and in vivo data observed for HK6a E2mc3-v1, which bears an H77 tVR2, suggests that tVR2 must be redesigned for each HCV isolate in the vaccine. Second, despite the poor yield and purity when displaying HK6a E2mc3-v1, the I3-01 constructs did show greater antigenicity than their E2p counterparts and could be produced in GMP CHO cells, suggesting that I3-01 may still be a valid nanoparticle display platform for HCV vaccine design, consistent with its outstanding immunogenicity in our previous HIV-1 vaccine study (*21*). In principle, one may expect a better immune response for HK6a E2 core nanoparticles with further optimization of HK6a E2mc3 and a more homogenous nanoparticle preparation. Other nanoparticles of bacterial origin, such as lumazine synthase and encapsulin (*25*, *56*, *57*), or from computational design (*58*), can also be used as multivalent carriers for optimized E2 cores. In addition, E2 cores of diverse genotypes can be displayed on synthetic lipid nanoparticles (*59*). Last, different adjuvants can be tested to ensure the optimal immune outcome. For example, an I3-01–based gp140 nanoparticle, when formulated with a Toll-like receptor 3 (TLR3) agonist, elicited rapid and potent NAb responses to a primary HIV-1 isolate in mice (*21*). Surface charge and hydrophobicity of the nanoparticle may affect the choice of adjuvant. Nevertheless, optimized E2 core nanoparticles derived from diverse genotypes, in a mixed form [cocktail or mosaic (*60*)] or sequentially, can now be used to generate rapid NAb response by targeting conserved E2 epitopes. Protection against HCV infection would also depend on the ability of these nanoparticle formulations to generate a long-term memory response, which has not been examined, however, in this proof-of-concept study. Durability of the NAb response, as well as other aspects of vaccine evaluation, will require further investigation in relevant animal models such as non-human primates with an extended immunization regimen.

MATERIALS AND METHODS

Structural design of tVR2

On the basis of the structure of bNAb AR3C-bound H77 E2c (*13*) (PDB ID: 4MWF), the already shortened VR2 loop in E2c, i.e., the segment between C452 and C494, was further truncated by manually removing exposed hydrophobic residues and a disulfide bond (C459-C486), resulting in H77 E2mc3 (fig. S1A). The tVR2 was modeled by LOOPY (*61*), a torsion-space loop modeling and prediction program. Computational redesign of tVR2 was then performed using an ensemble-based de novo protein design method (*38*) with a focus on the N-terminal region of the peptide sequence PERASGHYPRP between C452 and C494. Briefly, an ensemble of 11–amino acid (G_6HYPRP) or 10–amino acid (G_5HYPRP) loop conformations was generated to connect C452 and C494 using LOOPY (*61*). For each loop conformation, a starting sequence for the multiglycine (G_n) region was selected from a pool of 50 random sequences based on the RAPDF potential (*62*) and subjected to 500 steps of Monte Carlo simulated annealing (MCSA), with the temperature linearly decreasing from 300 to 10 K. The lowest energy sequence for each loop was recorded, and all MCSA-derived designs are ranked on the basis of energy at the completion of the process. The top five designs from the G_6 and G_5 ensembles, termed H77 E2mc3-v1-v5 and v6-v10, respectively, were selected for experimental validation. HK6a E2mc3 and E2mc3-v1 were designed by directly adopting the H77 sequence designs without further modification.

Expression and purification of E2 antigens

All E2 cores (E2c3, E2mc3, and E2mc3 v1-v10) and E2p-based nanoparticles were transiently expressed in HEK293 F cells (Thermo Fisher Scientific) for biochemical, biophysical, and antigenic analyses. Briefly, 293 F cells were thawed and incubated with FreeStyle 293 Expression Medium (Life Technologies, CA) in a shaker incubator at 37°C, 135 rpm, and 8% CO_2. When the cells reached a density of 2.0×10^6/ml, expression medium was added to reduce cell density to 1.0×10^6 ml^{-1} for transfection with polyethyleneimine (PEI) (Polysciences Inc). Next, 900 μg of plasmid in 25 ml of Opti-MEM transfection medium (Life Technologies, CA) was mixed with 5 ml of PEI-MAX (1.0 mg/ml) in 25 ml of Opti-MEM. After 30-min incubation, the DNA-PEI-MAX complex was added to 1 liter of 293 F cells. Culture supernatants were harvested 5 days after transfection, clarified by centrifugation at 1800 rpm for 20 min, and filtered using a 0.45-μm filter (Thermo Fisher Scientific). E2 proteins were extracted from the supernatants using an AR3A antibody column as previously described (*13*, *34*). Bound proteins were eluted three times, each with 5 ml of 0.2 M glycine (pH 2.2), and neutralized with 0.5 ml of tris base (pH 9.0). The proteins were further purified by SEC on a Superdex 75 Increase 10/300 GL column (GE Healthcare) for E2 cores and on a Superose 6 10/300 GL column (GE Healthcare) for E2p nanoparticles. E2mc3-v1–attached FR and I3-01 nanoparticles were produced in ExpiCHO cells (Thermo Fisher Scientific). Briefly, ExpiCHO cells were thawed and incubated with ExpiCHO Expression Medium (Thermo Fisher Scientific) in a shaker incubator at 37°C, 135 rpm, and 8% CO_2. When the cells reached a density of 10×10^6 ml^{-1}, ExpiCHO Expression Medium was added to reduce cell density to 6×10^6 ml^{-1} for transfection. The ExpiFectamine CHO/plasmid DNA complexes were prepared for 100-ml transfection in ExpiCHO cells following the manufacturer's instructions. For these two nanoparticles, 100 μg of plasmid and 320 μl of ExpiFectamine CHO reagent were mixed in 7.7 ml of cold OptiPRO medium (Thermo Fisher Scientific). After the first feed on day 1, ExpiCHO cells were cultured in a shaker incubator at 33°C, 115 rpm, and 8% CO_2 following the Max Titer protocol with an additional feed on day 5 (Thermo Fisher Scientific). Culture supernatants were harvested 13 to 14 days after transfection, clarified by centrifugation at 4000 rpm

for 20 min, and filtered using a 0.45-μm filter (Thermo Fisher Scientific). The AR3A antibody column was used to extract E2mc3-attached nanoparticles from the supernatants, which was followed by SEC on a Superose 6 10/300 GL column. For E2 cores and nanoparticles, protein concentration was determined using UV_{280} absorbance with theoretical extinction coefficients.

Blue native polyacrylamide gel electrophoresis

HCV E2 core nanoparticles were analyzed by BN-PAGE and stained with Coomassie blue. The proteins were mixed with sample buffer and G250 loading dye and added to a 4 to 12% bis-tris NativePAGE gel (Life Technologies). BN-PAGE gels were run for 2.5 hours at 150 V using the NativePAGE running buffer (Life Technologies) according to the manufacturer's instructions.

Enzyme-linked immunosorbent assay

Each well of a Costar 96-well assay plate (Corning) was first coated with 50 μl of phosphate-buffered saline (PBS) containing 0.2 μg of the appropriate antigens. The plates were incubated overnight at 4°C and then washed five times with wash buffer containing PBS and 0.05% (v/v) Tween 20. Each well was then coated with 150 μl of a blocking buffer consisting of PBS, blotting-grade blocker (40 mg ml^{-1}; Bio-Rad), and 5% (v/v) fetal bovine serum (FBS). The plates were incubated with the blocking buffer for 1 hour at room temperature and then washed five times with wash buffer. In the mouse sample analysis, serum or plasma was diluted by 50-fold in the blocking buffer and subjected to a 10-fold dilution series. For each sample dilution, a total of 50-μl volume was added to the wells. Each plate was incubated for 1 hour at room temperature and then washed five times with wash buffer. A 1:2000 dilution of horseradish peroxidase–labeled goat anti-mouse IgG antibody (Jackson ImmunoResearch Laboratories) was then made in the wash buffer, with 50 μl of this diluted secondary antibody added to each well. The plates were incubated with the secondary antibody for 1 hour at room temperature and then washed five times with wash buffer. Last, the wells were developed with 50 μl of TMB (3,3', 5,5;-tetramethylbenzidine) (Life Sciences) for 3 to 5 min before stopping the reaction with 50 μl of 2 N sulfuric acid. The resulting plate readouts were measured at a wavelength of 450 nm. Notably, the week 2 serum binding did not reach the plateau (or saturation) to allow for accurate determination of EC_{50} titers. Nonetheless, the EC_{50} values calculated in Prism were used as a quantitative measure of antibody titers to facilitate the comparison of different vaccine groups at week 2.

Biolayer interferometry

The kinetics of E2 cores and nanoparticle binding to HCV-specific antibodies was measured using an Octet Red96 instrument (FortéBio, Pall Life Sciences). All assays were performed with agitation set to 1000 rpm in FortéBio 1× kinetic buffer. The final volume for all the solutions was 200 μl per well. Assays were performed at 30°C in solid black 96-well plates (Geiger Bio-One). Antibody in 1× kinetic buffer (5 μg ml^{-1}) was loaded onto the surface of anti-human Fc capture biosensors (AHC) for E2 cores and of anti-human Fc quantitation biosensors (AHQ) for nanoparticles for 300 s. A 60-s biosensor baseline step was applied before the analysis of the association of the antibody on the biosensor to the antigen in solution for 200 s. A twofold concentration gradient of antigen, starting at 3.57 μM for E2 cores and 52.08 nM for nanoparticles, depending on the size, was used in a titration series of six. The dissociation of the interaction was followed for 300 s. Correction of baseline drift was performed by subtracting the mean value of shifts recorded for a sensor loaded with antibody but not incubated with antigen and for a sensor without antibody but incubated with antigen. Octet data were processed by FortéBio's data acquisition software v.8.1. Experimental data were fitted with the binding equations describing a 2:1 interaction to achieve optimal fitting. Notably, E2mc3-v1 binding was also measured using AHQ to facilitate the comparison of antibody binding signals with nanoparticles.

Differential scanning calorimetry

Thermal melting curves of HCV E2 core glycoproteins were obtained with a MicroCal VP-Capillary calorimeter (Malvern). The purified E2 glycoproteins produced from 293S cells were buffer exchanged into 1× PBS and concentrated to 27 to 50 μM before analysis by the instrument. Melting was probed at a scan rate of 90°C $hour^{-1}$ from 25° to 110°C. Data processing, including buffer correction, normalization, and baseline subtraction, was conducted using the standardized protocol from the Origin 7.0 software.

Protein expression and purification for crystallization

The E2 constructs were expressed and purified as previously described (*13*, *34*). Fabs AR3A and AR3B were expressed and purified as previously described (*63*). The monoclonal antibodies (mAbs) were purified on a protein G affinity column followed by SEC using a Superdex 200 column (Pharmacia) in 50 mM NaCl and 20 mM tris-HCl (pH 7.2) buffer.

Crystallization and structural determination of HK6a E2c3–Fab E1–AR3A–protein G complex

The HK6a E2c3–Fab E1–AR3A complex was formed by overnight incubation of purified E2 and Fabs in a molar ratio of 1:1.2:1.25 (E2:Fab E1:Fab AR3A) at room temperature followed by SEC (Superdex 200) to remove unbound Fabs using 20 mM tris and 50 mM NaCl (pH 7.2) buffer. Crystallization experiments were performed on our high-throughput CrystalMation robotic system (Rigaku) at Scripps Research using the vapor diffusion sitting drop method (drop size, 0.3 μl) at 20°C and resulted in crystals that diffracted to ~5 Å. To improve crystal resolution, before the crystallization experiment, domain III of protein G (PDB entry: 1IGC) was added to the HK6a E2c3–Fab E1–AR3A complex in a molar ratio of 1:2 (complex:protein G). These experiments resulted in crystals of HK6a E2c3–Fab E1–AR3A–protein G that diffracted to 3.40 Å (table S1) from a reservoir solution of 0.2 M magnesium chloride, 10% (w/v) polyethylene glycol (PEG) 3000, 15% ethylene glycol, and 0.1 M Na-cacodylate (pH 6.5). Before data collection, crystals were flash-cooled in liquid nitrogen. Diffraction datasets were collected at Stanford Synchrotron Radiation Lightsource (SSRL) (table S1). Data were integrated and scaled using HKL2000 (*64*), and the structure was solved by molecular replacement method using Phaser (*65*) with HK6a E2c3–AR3A (PDB entry: 6BKB) as a search model. Structure refinement was carried out in Phenix (*66*) and model building with COOT (*67*). Final refinement statistics are summarized in table S1.

Crystallization and structural determination of E2mc3-Fab complexes

Crystallization experiments were performed for H77 E2mc3, H77 E2mc3v-1, H77 E2mc3v-6, HK6a E2mc3, and HK6a E2mc3v-1 in

complex with AR3A, AR3B, AR3C, and AR3D Fabs. The E2-Fab complexes were formed by overnight incubation of purified E2 and Fabs in a molar ratio of 1:1.25 (E2:Fab) at room temperature followed by SEC (Superdex 200) to remove unbound Fabs using 20 mM tris and 50 mM NaCl (pH 7.2) buffer. Crystallization screening was again performed on our high-throughput CrystalMation robotic system (Rigaku) using the vapor diffusion sitting drop method (drop size, 0.3 μl) at 20°C, and crystals of H77 E2mc3-v1–AR3C, H77 E2mc3-v6–AR3C, and HK6a E2mc3-v1–AR3B were formed that diffracted to 1.90, 2.85, and 2.06 Å, respectively (table S2). Crystals of the H77 E2mc3-v1–AR3C complex were obtained using a reservoir solution of 20% (w/v) PEG 3500 and 0.2 M di-ammonium hydrogen phosphate, H77 E2mc3-v6–AR3C complex from 20% (w/v) PEG 3500 and 0.2 M Na-thiocyanate (pH 6.9), and HK6a E2mc3-v1–AR3B complex from 20% (w/v) PEG 8000 and 0.1 M Hepes (pH 7.5). Before data collection, H77 E2mc3-v6–AR3C and HK6a E2mc3-v1–AR3B crystals were cryoprotected with 10 to 15% ethylene glycol and flash-cooled in liquid nitrogen. Diffraction datasets were collected at the Advanced Photon Source (APS) (table S2). Data were integrated and scaled using HKL2000 (*64*). Structures were solved by molecular replacement method using Phaser (*65*) with H77 E2c–AR3C or HK6a E2c3–AR3B (PDB entry: 4MWF or 6BKC) as a search model. Structure refinement was carried out in Phenix (*66*) and model building with COOT (*67*). Final refinement statistics are summarized in table S2.

Negative-stain electron microscopy

The nsEM experiments were conducted at the Scripps Core Microscopy Facility. Briefly, nanoparticle samples were prepared at the concentration of 0.01 mg/ml. Carbon-coated copper grids (400 mesh) were glow-discharged, and 8 μl of each sample was adsorbed for 2 min. Excess sample was wicked away, and grids were negatively stained with 2% uranyl formate for 2 min. Excess stain was wicked away, and the grids were allowed to dry. Samples were analyzed at 80 kV with a Talos L120C transmission electron microscope (Thermo Fisher Scientific), and images were acquired with a CETA 16M complementary metal-oxide semiconductor (CMOS) camera.

Mouse immunization and sample collection

The Institutional Animal Care and Use Committee (IACUC) guidelines were followed with animal subjects tested in the immunization study. Eight-week-old BALB/c mice were purchased from The Jackson Laboratory. Mice were housed in ventilated cages in environmentally controlled rooms at Scripps Research, in compliance with an approved IACUC protocol and AAALAC (The Association for Assessment and Accreditation of Laboratory Animal Care International) guidelines. Mice were immunized at weeks 0, 3, 6, and 9 for a total of four times. Each immunization consisted of 200 μl of antigen/adjuvant mix containing 50 μg of vaccine antigen and 100 μl of AddaVax adjuvant (InvivoGen) via the subcutaneous route. Notably, to create the nanoparticle cocktail, equal amounts of H77 and HK6a E2mc3-v1-10GS-E2p nanoparticles, 25 μg each, were mixed before formulation with AddaVax. Because H77 and HK6a E2 cores have almost identical MWs, the mixing protocol ensures an approximate 1:1 molar ratio. Blood was collected 2 weeks after each immunization. All bleeds were performed through the facial vein (submandibular bleeding) using lancets (Goldenrod). While intermediate bleeds were collected without anticoagulant, terminal bleeds were collected using EDTA-coated tubes. Serum and plasma were heat-inactivated at 56°C for 30 min, spun at 1000 rpm for 10 min, and sterile-filtered. The cells were washed once in PBS and then resuspended in 1 ml of ACK red blood cell lysis buffer (Lonza). After two rounds of washing with PBS, peripheral blood mononuclear cells (PBMCs) were resuspended in 2 ml of Bambanker Freezing Media (Lymphotec). In addition, spleens were also harvested and grounded against a 70-μm cell strainer (BD Falcon) to release the splenocytes into a cell suspension. Splenocytes were centrifuged, washed in PBS, treated with 5 ml of Red Blood Cell Lysis Buffer Hybri-Max (Sigma-Aldrich), and frozen with 10% of dimethyl sulfoxide in FBS. While serum and plasma were used in HCV neutralization assays, 80% of the plasma from individual mice at week 11 in study #1 (9, 10, and 10 in groups 1, 2, and 3, respectively) were purified using a 0.2-ml Protein G Spin kit (Thermo Fisher Scientific) following the manufacturer's instructions. Purified IgGs were used to assess the polyclonal NAb response in HCV neutralization assays.

HCV neutralization assay

HCVpp assays were used to assess the neutralizing activity of vaccine-induced antibody response in mouse sera, purified mouse IgGs, and a control antibody panel. Briefly, HCVpps were generated by cotransfection of 293T cells with pNL4-3.lucR-E- plasmid and the corresponding expression plasmids encoding the E1E2 genes at a 4:1 ratio by polyethyleneimine as previously described (*36*). In vitro neutralization was carried on Huh7.5 cells using a single dilution of 1:50 for mouse sera and three concentrations (10, 1.0, and 0.1 μg/ml) for antibodies. In serum neutralization assays, each sample was tested in duplicate and the means of percent neutralization was calculated. Statistical comparison of different vaccine groups was performed using an unpaired, two-tailed Student's *t* test. Full neutralization curves were determined for IgGs purified from mice in study #1 against autologous H77 (1a) and heterologous SA13 (5a), with a starting IgG concentration of 100 μg/ml and a series of three-fold dilutions. As a negative control, pseudoparticles displaying the envelope glycoproteins of lymphocytic choriomeningitis virus (LCMVpps) were also tested in IgG neutralization following the same protocol. Due to the limited amount of IgG obtained from mouse sera, the IgG neutralization assays were performed without duplicate. For the control antibody panel, each of the six antibodies was tested at three concentrations (0.1, 1.0, and 10 mg/ml) in four separate neutralization experiments.

Bulk sorting of HCV E2–specific mouse B cells

Spleens were harvested from immunized mice 15 days after the last immunization, and cell suspension was prepared. Cells were stained as follows: Dead cells were excluded by staining with a Fixable Aqua Dead Cell Stain kit (Thermo Fisher Scientific, L34957). Receptors FcγIII (CD16) and FcγII (CD32) were blocked by adding 20 μl of 2.4G2 mAb (BD Pharmingen N553142). Cells were then incubated with biotinylated HCV E2mc3 protein (10 μg/ml). Briefly, E2mc3 was generated by biotinylation of the individual Avi-tagged HCV E2mc3 using biotin ligase BirA according to the manufacturer's instructions (Avidity LLC). Biotin excess was removed by SEC on a Superdex 200 column (GE Healthcare). In the SEC profile, the Avi-tagged E2mc3 peak is centered at 14.5 ml, while a broader peak of biotin ligase can be found at 18 to 23 ml. Cells and biotinylated proteins were incubated for 5 min at 4°C, followed by the addition of 2.5 μl of anti-mouse IgG fluorescently labeled with fluorescein isothiocyanate (FITC) (Jackson ImmunoResearch, 115-095-071), and incubated for 15 min at 4°C. Last, 5 μl of premium-grade allophycocyanin

(APC)–labeled streptavidin was added to the cells and incubated for 15 min at 4°C. In each step, cells were washed with Dulbecco's PBS, and the sorting buffer was 0.5 ml of fluorescence-activated cell sorting (FACS) buffer. $FITC^+$ APC^+ E2mc3–specific B cells were sorted using BD FACSAria II into Eppendorf tube with 500 μl of FACS buffer.

NGS and bioinformatics analysis of mouse B cells

A 5′-rapid amplification of complementary DNA (cDNA) ends (RACE) protocol has been reported for unbiased sequencing of mouse B cell repertoires (*21*, *24*). Here, this protocol was applied to bulk-sorted, E2-specific mouse splenic B cells. Briefly, 5′-RACE cDNA was obtained from bulk-sorted splenic B cells of each mouse with the SMART-Seq v4 Ultra Low Input RNA Kit for Sequencing (TaKaRa). The Ig polymerase chain reactions (PCRs) were set up with Platinum Taq High-Fidelity DNA Polymerase (Life Technologies) in a total volume of 50 μl, with 5 μl of cDNA as template, 1 μl of 5′-RACE primer, and 1 μl of 10 μM reverse primer. The 5′-RACE primer contained a PGM/S5 P1 adaptor, while the reverse primer contained a PGM/S5 A adaptor. We adapted the mouse 3′-C_γ1-3/3′-C_μ inner primers and 3′-mC_κ outer primer as reverse primers for 5′-RACE PCR processing of heavy and light (κ) chains. A total of 25 cycles of PCR was performed, and the expected PCR products (500 to 600 base pairs) were gel-purified (Qiagen). NGS was performed on the Ion S5 GeneStudio system. Briefly, heavy and light (κ) chain libraries from the same mouse were quantitated using Qubit 2.0 Fluorometer with the Qubit dsDNA HS Assay Kit and then mixed using a ratio of 3:1 before being pooled with antibody libraries of other mice at an equal ratio for sequencing. Template preparation and (Ion 530) chip loading were performed on Ion Chef using the Ion 520/530 Ext Kit, followed by sequencing on the Ion S5 system with default settings. The mouse antibodyomics pipeline (*24*) was used to process the raw data and determine distributions for germline gene usage, SHM, germline divergence, and HCDR3/KCDR3 loop length.

SUPPLEMENTARY MATERIALS

Supplementary material for this article is available at http://advances.sciencemag.org/cgi/content/full/6/16/eaaz6225/DC1

View/request a protocol for this paper from *Bio-protocol*.

REFERENCES AND NOTES

1. World Health Organization, *New Hepatitis Data Highlight Need for Urgent Global Response* (World Health Organization, 2017); www.who.int/hepatitis/publications/global-hepatitis-report2017/en/.
2. J. E. Zibbell, A. K. Asher, R. C. Patel, B. Kupronis, K. Iqbal, J. W. Ward, D. Holtzman, Increases in acute hepatitis C virus infection related to a growing opioid epidemic and associated injection drug use, United States, 2004 to 2014. *Am. J. Public Health* **108**, 175–181 (2018).
3. J.-M. Pawlotsky, J. J. Feld, S. Zeuzem, J. H. Hoofnagle, From non-A, non-B hepatitis to hepatitis C virus cure. *J. Hepatol.* **62**, S87–S99 (2015).
4. M. Thursz, A. Fontanet, HCV transmission in industrialized countries and resource-constrained areas. *Nat. Rev. Gastroenterol. Hepatol.* **11**, 28–35 (2014).
5. F. Conti, F. Buonfiglioli, A. Scuteri, C. Crespi, L. Bolondi, P. Caraceni, F. G. Foschi, M. Lenzi, G. Mazzella, G. Verucchi, P. Andreone, S. Brillanti, Early occurrence and recurrence of hepatocellular carcinoma in HCV-related cirrhosis treated with direct-acting antivirals. *J. Hepatol.* **65**, 727–733 (2016).
6. M. A. Konerman, A. S. Lok, Hepatitis C treatment and barriers to eradication. *Clin. Transl. Gastroenterol.* **7**, e193 (2016).
7. Centers for Disease Control and Prevention, *Surveillance for Viral Hepatitis—United States 2017* (Centers for Disease Control and Prevention, 2018); www.cdc.gov/hepatitis/statistics/2017surveillance/index.htm.
8. D. B. Smith, J. Bukh, C. Kuiken, A. S. Muerhoff, C. M. Rice, J. T. Stapleton, P. Simmonds, A web resource to manage the classification and genotype and subtype assignments of hepatitis C virus (2017); https://talk.ictvonline.org/ictv_wikis/flaviviridae/w/sg_flavi/56/hcv-classification.
9. P. Farci, New insights into the HCV quasispecies and compartmentalization. *Semin. Liver Dis.* **31**, 356–374 (2011).
10. B. D. Lindenbach, C. M. Rice, The ins and outs of hepatitis C virus entry and assembly. *Nat. Rev. Microbiol.* **11**, 688–700 (2013).
11. L. Fénéant, S. Levy, L. Cocquerel, CD81 and hepatitis C virus (HCV) infection. *Viruses* **6**, 535–572 (2014).
12. J. K. Ball, A. W. Tarr, J. A. McKeating, The past, present and future of neutralizing antibodies for hepatitis C virus. *Antiviral Res.* **105**, 100–111 (2014).
13. L. Kong, E. Giang, T. Nieusma, R. U. Kadam, K. E. Cogburn, Y. Hua, X. Dai, R. L. Stanfield, D. R. Burton, A. B. Ward, I. A. Wilson, M. Law, Hepatitis C virus E2 envelope glycoprotein core structure. *Science* **342**, 1090–1094 (2013).
14. A. G. Khan, J. Whidby, M. T. Miller, H. Scarborough, A. V. Zatorski, A. Cygan, A. A. Price, S. A. Yost, C. D. Bohannon, J. Jacob, A. Grakoui, J. Marcotrigiano, Structure of the core ectodomain of the hepatitis C virus envelope glycoprotein 2. *Nature* **509**, 381–384 (2014).
15. T. R. Fuerst, B. G. Pierce, Z. Y. Keck, S. K. H. Foung, Designing a B cell-based vaccine against a highly variable hepatitis C virus. *Front. Microbiol.* **8**, 2692 (2017).
16. C. Fauvelle, C. C. Colpitts, Z. Y. Keck, B. G. Pierce, S. K. Foung, T. F. Baumert, Hepatitis C virus vaccine candidates inducing protective neutralizing antibodies. *Expert Rev. Vaccines* **15**, 1535–1544 (2016).
17. D. W. Kulp, W. R. Schief, Advances in structure-based vaccine design. *Curr. Opin. Virol.* **3**, 322–331 (2013).
18. L. He, J. Zhu, Computational tools for epitope vaccine design and evaluation. *Curr. Opin. Virol.* **11**, 103–112 (2015).
19. R. W. Sanders, J. P. Moore, Native-like Env trimers as a platform for HIV-1 vaccine design. *Immunol. Rev.* **275**, 161–182 (2017).
20. A. B. Ward, I. A. Wilson, The HIV-1 envelope glycoprotein structure: Nailing down a moving target. *Immunol. Rev.* **275**, 21–32 (2017).
21. L. He, S. Kumar, J. D. Allen, D. Huang, X. Lin, C. J. Mann, K. L. Saye-Francisco, J. Copps, A. Sarkar, G. S. Blizard, G. Ozorowski, D. Sok, M. Crispin, A. B. Ward, D. Nemazee, D. R. Burton, I. A. Wilson, J. Zhu, HIV-1 vaccine design through minimizing envelope metastability. *Sci. Adv.* **4**, eaau6769 (2018).
22. L. He, N. de Val, C. D. Morris, N. Vora, T. C. Thinnes, L. Kong, P. Azadnia, D. Sok, B. Zhou, D. R. Burton, I. A. Wilson, D. Nemazee, A. B. Ward, J. Zhu, Presenting native-like trimeric HIV-1 antigens with self-assembling nanoparticles. *Nat. Commun.* **7**, 12041 (2016).
23. K. Sliepen, G. Ozorowski, J. A. Burger, T. van Montfort, M. Stunnenberg, C. LaBranche, D. C. Montefiori, J. P. Moore, A. B. Ward, R. W. Sanders, Presenting native-like HIV-1 envelope trimers on ferritin nanoparticles improves their immunogenicity. *Retrovirology* **12**, 82 (2015).
24. C. D. Morris, P. Azadnia, N. de Val, N. Vora, A. Honda, E. Giang, K. Saye-Francisco, Y. Cheng, X. Lin, C. J. Mann, J. Tang, D. Sok, D. R. Burton, M. Law, A. B. Ward, L. He, J. Zhu, Differential antibody responses to conserved HIV-1 neutralizing epitopes in the context of multivalent scaffolds and native-like gp140 trimers. *mBio* **8**, e00036-17 (2017).
25. M. Kanekiyo, W. Bu, M. G. Joyce, G. Meng, J. R. R. Whittle, U. Baxa, T. Yamamoto, S. Narpala, J.-P. Todd, S. S. Rao, A. B. McDermott, R. A. Koup, M. G. Rossmann, J. R. Mascola, B. S. Graham, J. I. Cohen, G. J. Nabel, Rational design of an Epstein-Barr virus vaccine targeting the receptor-binding site. *Cell* **162**, 1090–1100 (2015).
26. L. He, Y. Cheng, L. Kong, P. Azadnia, E. Giang, J. Kim, M. R. Wood, I. A. Wilson, M. Law, J. Zhu, Approaching rational epitope vaccine design for hepatitis C virus with meta-server and multivalent scaffolding. *Sci. Rep.* **5**, 12501 (2015).
27. B. G. Pierce, E. N. Boucher, K. H. Piepenbrink, M. Ejemel, C. A. Rapp, W. D. Thomas Jr., E. J. Sundberg, Z. Weng, Y. Wang, Structure-based design of hepatitis C virus vaccines that elicit neutralizing antibody responses to a conserved epitope. *J. Virol.* **91**, e01032-17 (2017).
28. A. Sandomenico, A. Leonardi, R. Berisio, L. Sanguigno, G. Focà, A. Focà, A. Ruggiero, N. Doti, L. Muscariello, D. Barone, C. Farina, A. Owsianka, L. Vitagliano, A. H. Patel, M. Ruvo, Generation and characterization of monoclonal antibodies against a cyclic variant of hepatitis C virus E2 epitope 412-422. *J. Virol.* **90**, 3745–3759 (2016).
29. A. I. Flyak, S. Ruiz, M. D. Colbert, T. Luong, J. E. Crowe Jr., J. R. Bailey, P. J. Bjorkman, HCV broadly neutralizing antibodies use a CDRH3 disulfide motif to recognize an E2 glycoprotein site that can be targeted for vaccine design. *Cell Host Microbe* **24**, 703–716. e703 (2018).
30. L. Kong, D. E. Lee, R. U. Kadam, T. Liu, E. Giang, T. Nieusma, F. Garces, N. Tzarum, V. L. Woods Jr., A. B. Ward, S. Li, I. A. Wilson, M. Law, Structural flexibility at a major conserved antibody target on hepatitis C virus E2 antigen. *Proc. Natl. Acad. Sci. U.S.A.* **113**, 12768–12773 (2016).
31. A. Goffard, J. Dubuisson, Glycosylation of hepatitis C virus envelope proteins. *Biochimie* **85**, 295–301 (2003).
32. E. Scarselli, H. Ansuini, R. Cerino, R. M. Roccasecca, S. Acali, G. Filocamo, C. Traboni, A. Nicosia, R. Cortese, A. Vitelli, The human scavenger receptor class B type I is a novel candidate receptor for the hepatitis C virus. *EMBO J.* **21**, 5017–5025 (2002).

33. J. Prentoe, R. Velazquez-Moctezuma, S. K. Foung, M. Law, J. Bukh, Hypervariable region 1 shielding of hepatitis C virus is a main contributor to genotypic differences in neutralization sensitivity. *Hepatology* **64**, 1881–1892 (2016).
34. N. Tzarum, E. Giang, L. Kong, L. He, J. Prentoe, E. Augestad, Y. Hua, S. Castillo, G. M. Lauer, J. Bukh, J. Zhu, I. A. Wilson, M. Law, Genetic and structural insights into broad neutralization of hepatitis C virus by human V_H1-69 antibodies. *Sci. Adv.* **5**, eaav1882 (2019).
35. N. Tzarum, I. A. Wilson, M. Law, The neutralizing face of hepatitis C virus E2 envelope glycoprotein. *Front. Immunol.* **9**, 1315 (2018).
36. M. Law, T. Maruyama, J. Lewis, E. Giang, A. W. Tarr, Z. Stamataki, P. Gastaminza, F. V. Chisari, I. M. Jones, R. I. Fox, J. K. Ball, J. A. McKeating, N. M. Kneteman, D. R. Burton, Broadly neutralizing antibodies protect against hepatitis C virus quasispecies challenge. *Nat. Med.* **14**, 25–27 (2008).
37. J. R. Bailey, J. R. Bailey, A. I. Flyak, V. J. Cohen, H. Li, L. N. Wasilewski, A. E. Snider, S. Wang, G. H. Learn, N. Kose, L. Loerinc, R. Lampley, A. L. Cox, J. M. Pfaff, B. J. Doranz, G. M. Shaw, S. C. Ray, J. E. Crowe Jr., Broadly neutralizing antibodies with few somatic mutations and hepatitis C virus clearance. *JCI Insight* **2**, 92872 (2017).
38. L. Kong, L. He, N. de Val, N. Vora, C. D. Morris, P. Azadnia, D. Sok, B. Zhou, D. R. Burton, A. B. Ward, I. A. Wilson, J. Zhu, Uncleaved prefusion-optimized gp140 trimers derived from analysis of HIV-1 envelope metastability. *Nat. Commun.* **7**, 12040 (2016).
39. Z.-Y. Keck, B. G. Pierce, P. Lau, J. Lu, Y. Wang, A. Underwood, R. A. Bull, J. Prentoe, R. Velázquez-Moctezuma, M. R. Walker, F. Luciani, J. D. Guest, C. Fauvelle, T. F. Baumert, J. Bukh, A. R. Lloyd, S. K. H. Foung, Broadly neutralizing antibodies from an individual that naturally cleared multiple hepatitis C virus infections uncover molecular determinants for E2 targeting and vaccine design. *PLOS Pathog.* **15**, e1007772 (2019).
40. G. T. Jennings, M. F. Bachmann, The coming of age of virus-like particle vaccines. *Biol. Chem.* **389**, 521–536 (2008).
41. N. Kushnir, S. J. Streatfield, V. Yusibov, Virus-like particles as a highly efficient vaccine platform: Diversity of targets and production systems and advances in clinical development. *Vaccine* **31**, 58–83 (2012).
42. J. D. Bazzill, L. J. Ochyl, E. Giang, S. Castillo, M. Law, J. J. Moon, Interrogation of antigen display on individual vaccine nanoparticles for achieving neutralizing antibody responses against hepatitis C virus. *Nano Lett.* **18**, 7832–7838 (2018).
43. Y. Yan, X. Wang, P. Lou, Z. Hu, P. Qu, D. Li, Q. Li, Y. Xu, J. Niu, Y. He, J. Zhong, Z. Huang, A nanoparticle-based HCV vaccine with enhanced potency. *J. Infect. Dis.* jiz228 (2019).
44. E. C. Theil, Ferritin: Structure, gene regulation, and cellular function in animals, plants, and microorganisms. *Annu. Rev. Biochem.* **56**, 289–315 (1987).
45. P. D. Griffiths, A. Stanton, E. McCarrell, C. Smith, M. Osman, M. Harber, A. Davenport, G. Jones, D. C. Wheeler, J. O'Beirne, D. Thorburn, D. Patch, C. E. Atkinson, S. Pichon, P. Sweny, M. Lanzman, E. Woodford, E. Rothwell, N. Old, R. Kinyanjui, T. Haque, S. Atabani, S. Luck, S. Prideaux, R. S. Milne, V. C. Emery, A. K. Burroughs, Cytomegalovirus glycoprotein-B vaccine with MF59 adjuvant in transplant recipients: A phase 2 randomised placebo-controlled trial. *Lancet* **377**, 1256–1263 (2011).
46. S. E. Frey, M. Houghton, S. Coates, S. Abrignani, D. Chien, D. Rosa, P. Pileri, R. Ray, A. M. Di Bisceglie, P. Rinella, H. Hill, M. C. Wolff, V. Schultze, J. H. Han, B. Scharschmidt, R. B. Belshe, Safety and immunogenicity of HCV E1E2 vaccine adjuvanted with MF59 administered to healthy adults. *Vaccine* **28**, 6367–6373 (2010).
47. X. Wu, Z. Y. Yang, Y. Li, C. M. Hogerkorp, W. R. Schief, M. S. Seaman, T. Zhou, S. D. Schmidt, L. Wu, L. Xu, N. S. Longo, K. McKee, S. O'Dell, M. K. Louder, D. L. Wycuff, Y. Feng, M. Nason, N. Doria-Rose, M. Connors, P. D. Kwong, M. Roederer, R. T. Wyatt, G. J. Nabel, J. R. Mascola, Rational design of envelope identifies broadly neutralizing human monoclonal antibodies to HIV-1. *Science* **329**, 856–861 (2010).
48. K. F. Dai, L. He, S. N. Khan, S. O'Dell, K. McKee, K. Tran, Y. Li, C. Sundling, C. D. Morris, J. R. Mascola, G. B. Karlsson Hedestam, R. T. Wyatt, J. Zhu, Rhesus macaque B-cell responses to an HIV-1 trimer vaccine revealed by unbiased longitudinal repertoire analysis. *mBio* **6**, e01375-15 (2015).
49. J. K. Hu, J. C. Crampton, A. Cupo, T. Ketas, M. J. van Gils, K. Sliepen, S. W. de Taeye, D. Sok, G. Ozorowski, I. Deresa, R. Stanfield, A. B. Ward, D. R. Burton, P. J. Klasse, R. W. Sanders, J. P. Moore, S. Crotty, Murine antibody responses to cleaved soluble HIV-1 envelope trimers are highly restricted in specificity. *J. Virol.* **89**, 10383–10398 (2015).
50. Z. -Y. Keck, J. Xia, Y. Wang, W. Wang, T. Krey, J. Prentoe, T. Carlsen, A. Y.-J. Li, A. H. Patel, S. M. Lemon, J. Bukh, F. A. Rey, S. K. H. Foung, Human monoclonal antibodies to a novel cluster of conformational epitopes on HCV E2 with resistance to neutralization escape in a genotype 2a isolate. *PLOS Pathog.* **8**, e1002653 (2012).
51. L. Kong, E. Giang, J. B. Robbins, R. L. Stanfield, D. R. Burton, I. A. Wilson, M. Law, Structural basis of hepatitis C virus neutralization by broadly neutralizing antibody HCV1. *Proc. Natl. Acad. Sci. U.S.A.* **109**, 9499–9504 (2012).
52. Z. Keck, W. Wang, Y. Wang, P. Lau, T. H. Carlsen, J. Prentoe, J. Xia, A. H. Patel, J. Bukh, S. K. Foung, Cooperativity in virus neutralization by human monoclonal antibodies to two adjacent regions located at the amino terminus of hepatitis C virus E2 glycoprotein. *J. Virol.* **87**, 37–51 (2012).
53. N. H. Shoukry, Hepatitis C vaccines, antibodies, and T cells. *Front. Immunol.* **9**, 1480 (2018).
54. M. L. Keck, F. Wrensch, B. G. Pierce, T. F. Baumert, S. K. H. Foung, Mapping determinants of virus neutralization and viral escape for rational design of a hepatitis C virus vaccine. *Front. Immunol.* **9**, 1194 (2018).
55. F. Chen, N. Tzarum, I. A. Wilson, M. Law, V_H1-69 antiviral broadly neutralizing antibodies: Genetics, structures, and relevance to rational vaccine design. *Curr. Opin. Virol.* **34**, 149–159 (2019).
56. J. G. Jardine, T. Ota, D. Sok, M. Pauthner, D. W. Kulp, O. Kalyuzhniy, P. D. Skog, T. C. Thinnes, D. Bhullar, B. Briney, S. Menis, M. Jones, M. Kubitz, S. Spencer, Y. Adachi, D. R. Burton, W. R. Schief, D. Nemazee, Priming a broadly neutralizing antibody response to HIV-1 using a germline-targeting immunogen. *Science* **349**, 156–161 (2015).
57. J. Jardine, J.-P. Julien, S. Menis, T. Ota, O. Kalyuzhniy, A. McGuire, D. Sok, P. S. Huang, S. MacPherson, M. Jones, T. Nieusma, J. Mathison, D. Baker, A. B. Ward, D. R. Burton, L. Stamatatos, D. Nemazee, I. A. Wilson, W. R. Schief, Rational HIV immunogen design to target specific germline B cell receptors. *Science* **340**, 711–716 (2013).
58. J. B. Bale, S. Gonen, Y. Liu, W. Sheffler, D. Ellis, C. Thomas, D. Cascio, T. O. Yeates, T. Gonen, N. P. King, D. Baker, Accurate design of megadalton-scale two-component icosahedral protein complexes. *Science* **353**, 389–394 (2016).
59. S. Bale, G. Goebrecht, A. Stano, R. Wilson, T. Ota, K. Tran, J. Ingale, M. B. Zwick, R. T. Wyatt, Covalent linkage of HIV-1 trimers to synthetic liposomes elicits improved B cell and antibody responses. *J. Virol.* **91**, e00443-17 (2017).
60. M. Kanekiyo, M. G. Joyce, R. A. Gillespie, J. R. Gallagher, S. F. Andrews, H. M. Yassine, A. K. Wheatley, B. E. Fisher, D. R. Ambrozak, A. Creanga, K. Leung, E. S. Yang, S. Boyoglu-Barnum, I. S. Georgiev, Y. Tsybovsky, M. S. Prabhakaran, H. Andersen, W. P. Kong, U. Baxa, K. L. Zephir, J. E. Ledgerwood, R. A. Koup, P. D. Kwong, A. K. Harris, A. B. McDermott, J. R. Mascola, B. S. Graham, Mosaic nanoparticle display of diverse influenza virus hemagglutinins elicits broad B cell responses. *Nat. Immunol.* **20**, 362–372 (2019).
61. Z. Xiang, C. S. Soto, B. Honig, Evaluating conformational free energies: The colony energy and its application to the problem of loop prediction. *Proc. Natl. Acad. Sci. U.S.A.* **99**, 7432–7437 (2002).
62. J. Zhu, L. Xie, B. Honig, Structural refinement of protein segments containing secondary structure elements: Local sampling, knowledge-based potentials, and clustering. *Proteins* **65**, 463–479 (2006).
63. E. Giang, M. Dorner, J. C. Prentoe, M. Dreux, M. J. Evans, J. Bukh, C. M. Rice, A. Ploss, D. R. Burton, M. Law, Human broadly neutralizing antibodies to the envelope glycoprotein complex of hepatitis C virus. *Proc. Natl. Acad. Sci. U.S.A.* **109**, 6205–6210 (2012).
64. Z. Otwinowski, W. Minor, Processing of X-ray diffraction data collected in oscillation mode. *Methods Enzymol.* **276**, 307–326 (1997).
65. A. J. McCoy, R. W. Grosse-Kunstleve, L. C. Storoni, R. J. Read, Likelihood-enhanced fast translation functions. *Acta Crystallogr. D Biol. Crystallogr.* **61**, 458–464 (2005).
66. P. D. Adams, R. W. Grosse-Kunstleve, L.-W. Hung, T. R. Ioerger, A. J. McCoy, N. W. Moriarty, R. J. Read, J. C. Sacchettini, N. K. Sauter, T. C. Terwilliger, *PHENIX*: Building new software for automated crystallographic structure determination. *Acta Crystallogr. D Biol. Crystallogr.* **58**, 1948–1954 (2002).
67. P. Emsley, K. Cowtan, *Coot*: Model-building tools for molecular graphics. *Acta Crystallogr. D Biol. Crystallogr.* **60**, 2126–2132 (2004).
68. Z.-Y. Keck, A. Saha, J. Xia, Y. Wang, P. Lau, T. Krey, F. A. Rey, S. K. H. Foung, Mapping a region of hepatitis C virus E2 that is responsible for escape from neutralizing antibodies and a core CD81-binding region that does not tolerate neutralization escape mutations. *J. Virol.* **85**, 10451–10463 (2011).
69. I. W. Davis, A. Leaver-Fay, V. B. Chen, J. N. Block, G. J. Kapral, X. Wang, L. W. Murray, W. B. Arendall III, J. Snoeyink, J. S. Richardson, D. C. Richardson, MolProbity: All-atom contacts and structure validation for proteins and nucleic acids. *Nucleic Acids Res.* **35**, W375–W383 (2007).

Acknowledgments: We thank Z. Keck and S. Foung at Stanford University for sharing of antibody reagents , and Juan Carlos de la Torre for the LCMV GP plasmid. We thank R. Stanfield, X. Dai, and M. Elsliger for crystallographic and computational support and H. Tien in the Wilson laboratory for automated crystal screening. X-ray datasets were collected at the APS beamline 23ID-B (GM/CA CAT) and SSRL beamline 12-2. **Funding:** This work was funded, in part, by HIV Vaccine Research and Design (HIVRAD) program (P01 AI124337 to J.Z.), NIH grants AI129698 and AI140844 (to J.Z.), UfoVax/SFP-2018-0416 and UfoVax/SFP-2018-1013 (to J.Z.), AI123861 (to M.L. and J.Z.), AI079031 (to M.L.), and AI123365 and AI106005 (to M.L. and I.A.W.). The use of the APS was supported by the U.S. Department of Energy (DOE), Basic Energy Sciences, Office of Science, under contract DE-AC02-06CH11357. The use of the SSRL Structural Molecular Biology Program was supported by DOE Office of Biological and Environmental Research and by the NIH NIGMS (including P41GM103393) and the National Center for Research Resources (P41RR001209). **Author contributions:** Project design: L.H., N.T., M.L., I.A.W., and J.Z.; structural design of E2 cores and E2 core nanoparticles: L.H. and J.Z.; plasmid design and processing: L.H. and C.S.; antigen production, purification, and

biochemical characterization: L.H., X.L., B.S., and C.J.M.; HCV antibody production: E.G., N.T., and M.L.; E2 complex crystallization, structure determination, and refinement: N.T. and I.A.W.; DSC measurement: N.T.; nsEM: L.H. and J.Z.; BLI of E2 cores and E2 core nanoparticles: L.H. and X.L.; mouse serum antigen ELISA: L.H. and X.L.; mouse serum neutralization: L.H., X.L., and K.N.; antigen-specific mouse B cell sorting: L.H. and L.Z.; mouse B cell sequencing: L.H., X.L., and J.Z.; bioinformatics analysis: L.H., X.L., and J.Z.; antibody neutralization: L.H. and X.L.; IgG purification: L.H. and C.S.; epitope mapping: L.H. and X.L.; manuscript writing: L.H., N.T., M.L., I.A.W., and J.Z. All authors were asked to comment on the manuscript. The TSRI manuscript number is 29867. **Competing interests:** L.H., J.Z., E.G., M.L., I.A.W., and N.T. are inventors on a patent application related to this work (no. 62/879,100, filed on 26 July 2019). The authors declare no other competing interests. **Data and materials availability:** All data and code needed to evaluate the conclusions in the paper are present in the paper and/or the Supplementary Materials. The x-ray coordinates and structure factors have been deposited to the PDB with accession codes 6UYD, 6UYF, 6UYM, and 6UYG. Additional data related to this paper may be requested from the corresponding authors.

Submitted 24 September 2019
Accepted 22 January 2020
Published 15 April 2020
10.1126/sciadv.aaz6225

Citation: L. He, N. Tzarum, X. Lin, B. Shapero, C. Sou, C. J. Mann, A. Stano, L. Zhang, K. Nagy, E. Giang, M. Law, I. A. Wilson, J. Zhu, Proof of concept for rational design of hepatitis C virus E2 core nanoparticle vaccines. *Sci. Adv.* **6**, eaaz6225 (2020).

Science Advances

Proof of concept for rational design of hepatitis C virus E2 core nanoparticle vaccines

Linling He, Netanel Tzarum, Xiaohe Lin, Benjamin Shapero, Cindy Sou, Colin J. Mann, Armando Stano, Lei Zhang, Kenna Nagy, Erick Giang, Mansun Law, Ian A. Wilson and Jiang Zhu

Sci Adv **6** (16), eaaz6225.
DOI: 10.1126/sciadv.aaz6225